We are IntechOpen, the world's leading publisher of Open Access books Built by scientists, for scientists

4,800
Open access books available

122,000
International authors and editors

135M
Downloads

154
Countries delivered to

Our authors are among the

TOP 1%
most cited scientists

12.2%
Contributors from top 500 universities

CLARIVATE ANALYTICS
BOOK CITATION INDEX
INDEXED

WEB OF SCIENCE™

Selection of our books indexed in the Book Citation Index
in Web of Science™ Core Collection (BKCI)

Interested in publishing with us?
Contact book.department@intechopen.com

Numbers displayed above are based on latest data collected.
For more information visit www.intechopen.com

Influence of Dopants, Temperature and Atmosphere of Sintered on the Microstructure and Behavior of Lead Free Ceramics

Maria A. Zaghete[1], Francisco Moura[2], Alexandre Z. Simões[3],
José A.Varela[1] and Elson Longo[1]
[1]*Instituto de Química, Universidade Estadual Paulista – UNESP –*
Campus de Araraquara (SP)
[2]*Universidade Estadual Paulista,UNESP, Campus de Guaratinguetá, SP*
[3]*Laboratório Interdisciplinar de Materiais Avançados, Universidade Federal de*
Itajubá,Unifei-Itabira, MG
Brasil

1. Introduction

Ceramics based on barium titanate ($BaTiO_3$) with modified electrical properties have been obtained by substitution of isovalent cations both in barium and titanium sites. Barium zirconium titanate solid solution has been widely researched owing to the diffusion phase transition characteristics caused by the substitution of Ti^{4+} for Zr^{4+}. It is well known that with increasing Zr^{4+} content the three transition points and the three corresponding ε_r maxima move closer together and finally coalesce into a single broad maximum (Nejman,1988; Hcnnings & Sehnell, 1982) . Undoped barium zirconium titanate ceramics, however, usually need a very high sintering temperature above 1400°C because of the slow diffusion velocity. Little amount of additives such as ZnO, CuO, and SiO_2 could greatly lower the sintering temperature by 100-300°C but cause the degradation of the dielectric properties at the same time owing to the deposition of vitreous phase along grain boundaries (Amador et al. 1998). It is well known that $BaTiO_3$ is cubic above 120-135 °C and belongs to the space group Pm3m (Oh1). At temperatures below 120 °C it is ferroelectric with P4mm (C4v1) structure, which further transforms to orthorhombic and rhombohedral structures at 5°C and -90 °C, respectively (Scott, 1974). The Curie temperature and the dielectric permittivity of barium titanate ($BaTiO_3$) can be adjusted in a large range in the $BaTiO_3$-$SrTiO_3$ solid solution (Miura et al., 1975; Bornstein, 1981).

Studies on the solid solution $BaTiO_3$-$BaZrO_3$ have shown some interesting characteristics in bulk materials (Ravez& Simon, 2000; Dobal et al., 2001). For example, in the $Ba[Ti_{(1-x)}Zr_x]O_3$ composition with x in the range $0.26 < x < 0.42$, the temperature dependence of the real part of the dielectric permittivity at the transition temperature is broad and frequency dependent (Ravez& Simon, 1999). The effect of doping on various physical and chemical properties of BZT is known, and this effect has been extensively exploited in piezoelectrics and ferroelectrics to improve their performance. Many aliovalent compositional alterations to BZT have been studied either with higher valence substitutions (donors), or with lower

valence ions (acceptors). Donor dopants, such as Va^{5+} and W^{6+}, induce cationic defects while occupying the B site of the perovskite lattice (Zhi et al., 2000; Moura et al., 2008). Such behavior may cause several effects on the dielectric behavior through interaction with domain walls (Shannigrahi et al. 1999; Bolten et al. 2000). Barium titanate compositions modified by Sn, Hf, Ce, Y and Zr (Payne& Tennery, 1965; Jing at al. 1998; . Yu et al. 2001) have been extensively studied for dielectric application and all exhibit a crossover from typical ferroelectric to ferroelectric-relaxor behavior at higher concentrations of substitution. Also was observed that remnant polarization and coercive field are affected by substitution due the electron-relaxation-mode in which carriers (polarons, protons, and so on) are coupled with existing dielectric modes. Dielectric relaxation in relaxor ferroelectrics has become a topic of considerable interest (Cross,1987; Cheng et al.1998; Tagantsev & Glazounov, 1998). To account for the relaxation phenomena two different approaches are commonly used. The traditional one, considers clusters of polar phase located in non-polar phase to be responsible for the unusual relaxation behavior. It was proposed that the relaxation polarization was attributed to the thermo activated reorientation of dipolar moments of clusters or the motion of the clusters boundaries (Smolensky et al. ,1984; Bovtoun & Leshchenko, 1997; Courtens, 1984). The second approach implies the existence of a structural (dipolar) glass state in relaxors. The literature reports the frequent use of impedance spectroscopy analyses to reveal and study the mechanisms responsible for the dielectric properties of polycrystalline materials (Sinclair et al.,2002; Fang & Shiau, 2004; West et al., 2004), particularly to obtain information on non intrinsic dielectric effects.

The purpose of using dielectric spectroscopy analysis instead of the traditional impedance spectroscopy approach is to demonstrate that dielectric complex diagrams of the frequency response of polycrystalline materials can sometimes reveal more about the relaxation processes involved with grain boundaries and dielectric dipolar relaxation than impedance diagrams can (Böttcher & Bordewijk, 1992; Jonscher,1990).

Although $BaTiO_3$ it is a well known lead-free ceramic, detailed ferroelectric and piezoelectric behavior was less studied although some piezoelectric properties has been reported (Kell & Hellicar,1956). On the other hand, the recent discovery about very high piezoelectric and electrostrictive properties of lead based relaxor ferroelectric single crystals (Park& Shrout,1997; Paik et al.,1999; Liu et al.1999) has stimulated a renewed interest in searching for high strain materials, especially environmentally friendly lead-free materials. It is known that doping is an effective way to improve the material performance in electroceramics. Zirconium doped $BaTiO_3$ single crystals were recently grown and show promising piezoelectric and electrostrictive properties (Rehrig et al., 1999; Zhi et al.2001, 2000) . In perovskites the relaxor behavior occurs mainly in lead-based compositions with more than one type of ion occupying the equivalent six coordinated crystallographic sites (Moura et al.,2008; Dmowski et al.,2002). In turn, the substitution of Ti^{4+} by Zr^{4+} promotes several interesting features in the dielectric behavior of Barium titanate ceramics. When the Zr content is less than 10 at.% the BZT ceramics show normal ferroelectric behavior and dielectric anomalies corresponding several phase transition: cubic to tetragonal (T1), tetragonal to orthorhombic (T2) and orthorhombic to rhombohedral (T3). The interest in high strain piezoelectric materials is increasing for electromechanical transducers and various related applications. $BaTiO_3$ (BTO) is known to have a large electromechanical coupling factor. The effect of doping on various physical and chemical properties of this material is known, and this effect has been extensively exploited in piezoelectric and ferroelectrics to improve their performance. Many aliovalent compositional alterations to

$Ba(Ti_{1-x}Zr_x)O_3$ have been studied either with higher valence substitutions (donors), or with lower valence ions (acceptors).

Recently, it was found that the solid solubility of Y doped $BaTiO_3$ could reach up to 12.2 mol% once yttrium ions have stable valence (Zhi et al., 2000). Donor dopant,such as W^{6+}, induces cationic defects while occupying the B site of the perovskite lattice (Carg & Goel, 1999; Shannigrahi et al.,1999). Such behaviour may cause several effects on the dielectric properties through interaction with domain walls (Bolten et al., 2000; Takahashi,1982). Most studies on $Ba(Ti_{1-x}Zr_x)O_3$ ceramics are focused on the temperature dependence of the dielectric permittivity and relaxor behaviour (Ravez & Simon,1997a; 1997b; Farhi et al., 1999). The DPT was found in solid solutions of $BaTiO_3$ and $BaZrO_3$ (BTZ) which is one of the most important compositions for dielectrics in multilayer ceramic capacitors (Hennings et al.,1982), because Zr ion has higher chemical stability than Ti (Hoffmann & Waser, 1999; Tsurumi et al., 2002) ion and the high permittivity of the $BaTiO_3$ ceramic is increased more by the addition of zirconium. The sintering temperature of BZT is 1400 °C, when Zr^{4+} is added the sintering temperature decrease and dielectric constant rising (Weber et al., 2001). When the ratio of Zr to Ti in BZT reaches 20%, the Curie temperature is at room temperature around 27C, which is the ideal material for preparing variable electric capacities (Hennings et al.,1982) . Chen suggested (Chen, 2000) that these features of the relaxor phenomena are not caused by elementary excitation or the typical dielectric sources, (space charge), but reminiscence of a broad first-order phase transition obscured by severe geometrical and compositional randomness. However, there are some theories considering the origin of high dielectric permittivity of relaxor as the space charges arise from defects or vacancies (Dixit et al.,2003; Wang et al.,2002). Ionic doping is a common method for optimizing the electric properties of ceramics. It is known that doping is an effective way to improve the material performance in electroceramics. Zr-doped $BaTiO_3$ single crystals were recently grown and show promising piezoelectric/electrostrictive properties (Rehrig et al.,1999; Zhi et al., 2001; 2000a; 2000b). Similarity to Zr modified BT, BZT:2W may be a promising material as lead free actuator. Because of that it is important to study and compreend how the properties of ceramics materials are significantly affected by temperature, defects, atmosphere flow. It is important to control the temperature due to its strong influence on the grain size, dielectric and ferroelectric properties (Tang et al., 2004; Simões et al., 2005; Marques et al.,2007). The medium and fine grained ceramics possess poor dielectric properties influencing the performance of the device. This is due the oxygen interdiffusion, chemical reaction, or structural defects in this particle size range . Properties of ceramic materials are significantly affected by temperature, defects, atmosphere flow. This is due to the oxygen interdiffusion, chemical reaction, or structural defects in this particle size range. In the present study, a deep investigation on temperature and concentration of vanadium and tungsten dependence of electrical properties of *BZT:10* ceramics prepared by mixed oxide method was performed. Due its better electrical properties BZT10:2V ceramics had their properties evaluated as a function of annealing atmosphere.

2. Influence of zirconium ions concentration on the crystal structure and electrical properties of the barium titanate ceramics

2.1 Preparation of solid solution BaTiO₃- BaZrO₃ by mixed oxide method

The addition of Zr strongly influenced the crystal structure and electrical properties of the barium titanate ceramics. The investigated systems were $Ba(Ti_{0.95}Zr_{0.05})O_3$, $Ba(Ti_{0.9}Zr_{0.10})O_3$

and $Ba(Ti_{0.85}Zr_{0.15})O_3$. In this study, barium zirconium titanate (BZT) ceramics were prepared by mixed oxide method. The powders were homogenized in a ball mill using isopropyl alcohol. All oxides were analytical grade: $BaCO_3$ (Vetec), ZrO_2 (Inlab), TiO_2 (Vetec). After drying, the powders were calcinated at 1200°C for 2 hours. After that powder were compacted in two steps, first by pressing one way then the pellets are pressed isostatically at 210 MPa, in the form of pellets with 6mm long and 8 mm of diameter to be
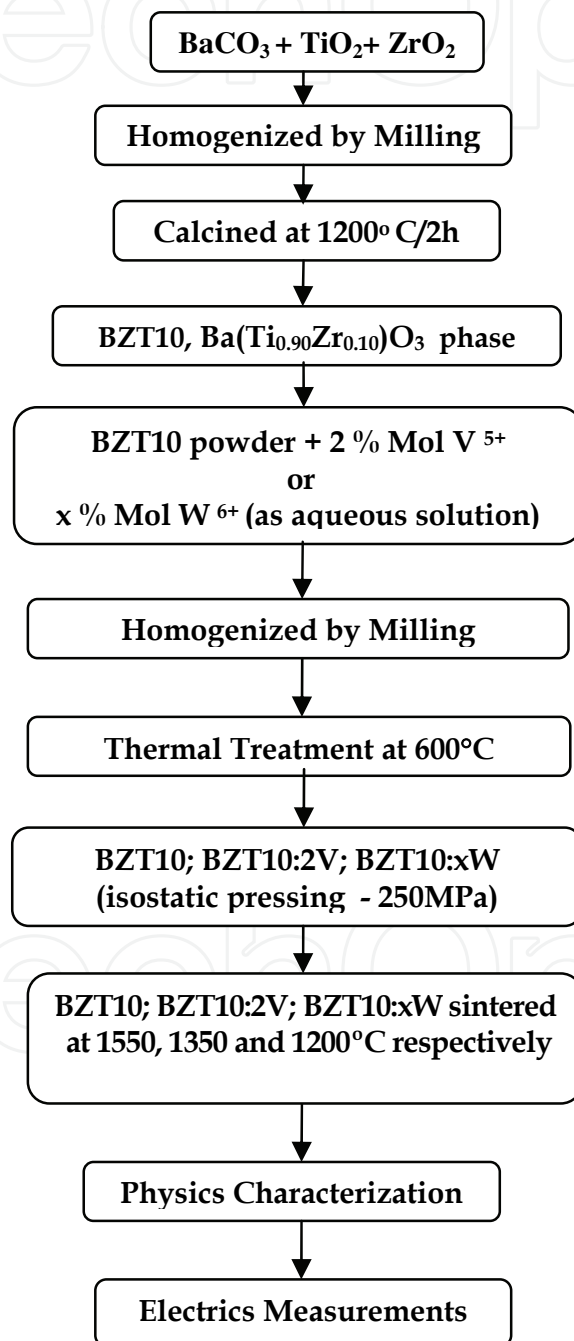
Fig. 1. Flowchart of the synthesis and characterization process of BZT10; BZT10:xV; BZT10:yW

submitted at dilatometric analyses. This mesurament were performed in a Nezstch dilatometer 402 E, up to 1550°C, at a heating rate of 5 °C/min in static atmosphere and the results of linear shrinkage rate $(d(\Delta l/l_0)/dT)$ and linear shrinkage $\Delta l/l_0$ were determined. Considering the results of linear shrinkage rate, new samples were obtained from powders calcined at 1200 °C. The powders were compacted in the form of pellets with 1 mm of thickness and 12 mm of diameter, isostatically pressed at 210MPa. The pellets were sintered at 1550°C for 4 hours in static air and cooled to room temperature (5 °C/min).

2.2 Preparation of solid solution BZT10:xV and BZT10:yW by mixed oxide method

The dopants, as aqueous complex, were added to the calcined powders at 1200°C as described. Separately, vanadium or tungsten oxides were dissolved in nitric acid and complexed with citric acid. After that, ethylene glycol was added in the medium to obtain the stable aqueous complex. A volume, which correspond to the concentration of vanadium or tungsten necessary to get BZT:yV or BZT:xW in molar ratio was added to BZT powders. The BZT10 powder wet with doping solution was homogenized by grinding, dried and calcined ate 600°C to eliminated all the organic material (citric acid and ethylene glycol from dopant solution). After this process, the powders were compacted in the form of pellets with 1 mm of thickness and 12 mm of diameter, isostatically pressed at 210MPa and sintered at 1350°C for different concentrations of dopants (BZT10:1V to BZT10:6V) and BZT10:2V at different temperatures.

2.3 Techniques used in the characterization of solid solution BZT10; BZT10:xV and BZT10:yW

X-ray diffraction data were collected with a Rigaku Rint 2000 diffractometer under the following experimental condition: 50 kV, 150 mA, 20°$\leq$ 2θ $\leq$ 80°, $\Delta 2\theta$ = 0.02°, λ_{Cu} k_α monocromatized by a graphite crystal, divergence slit = 2mm, reception slit = 0.6mm, step time = 10s. Raman measurements were performed using an ISAT 64000 triple monochromator. The samples also were characterized by dielectrics properties. Gold electrodes, for electrical measurements, were applied by evaporation through a sputtering system on polished surfaces of sintered discs. Ferroelectric properties were measured on a Radiant Technology RT6600A tester system equipped with a micrometer probe station in a virtual ground mode. The dielectric characterization was accomplished with HP 4192 impedance analyzer, and measurements of the capacitance as a function of temperature at a frequency of 10 kHz were performed. From the capacitance dependence temperature curves, the Curie temperature was determined. Piezoelectric measurements were carried out using a setup based on an atomic force microscope in a Multimode Scanning Probe Microscope with Nanoscope IV controller (Veeco FPP-100). In our experiments, piezoresponse images were acquired in ambient air by applying a small ac voltage with amplitude of 2.5 V (peak to peak) and a frequency of 10 kHz while scanning the sample surface. To apply the external voltage we used a standard gold coated Si_3N_4 cantilever with a spring constant of 0.09 N/m. The probing tip, with an apex radius of about 20 nm, was in mechanical contact with the uncoated samplesurface during the measurements. Cantilever vibration was detected using a conventional lock-in technique.

2.4 Results from characterization of the Ba(Ti$_{1-x}$ Zr$_x$)O$_3$ systems.

The X-ray diffraction crystal structure of the Ba(Ti$_{0.95}$Zr$_{0.05}$)O$_3$, Ba(Ti$_{0.9}$Zr$_{0.10}$)O$_3$ and Ba(Ti$_{0.85}$Zr$_{0.15}$)O$_3$ powders are represented in Figure 2 and show that all the ceramics

composition were crystallized into a single-phase perovskite structure. This is a clear indication that the addition of Zr is forming a stable solid solution with the $BaTiO_3$ lattice. As reported in other studies (Yu et al.,2002; Dixit, et al., 2003; Dobal et al., 2002; Paik et al., 1999) depending upon the Zr content, BZT may have orthorhombic, rhombohedral and tetragonal structures at room temperature.
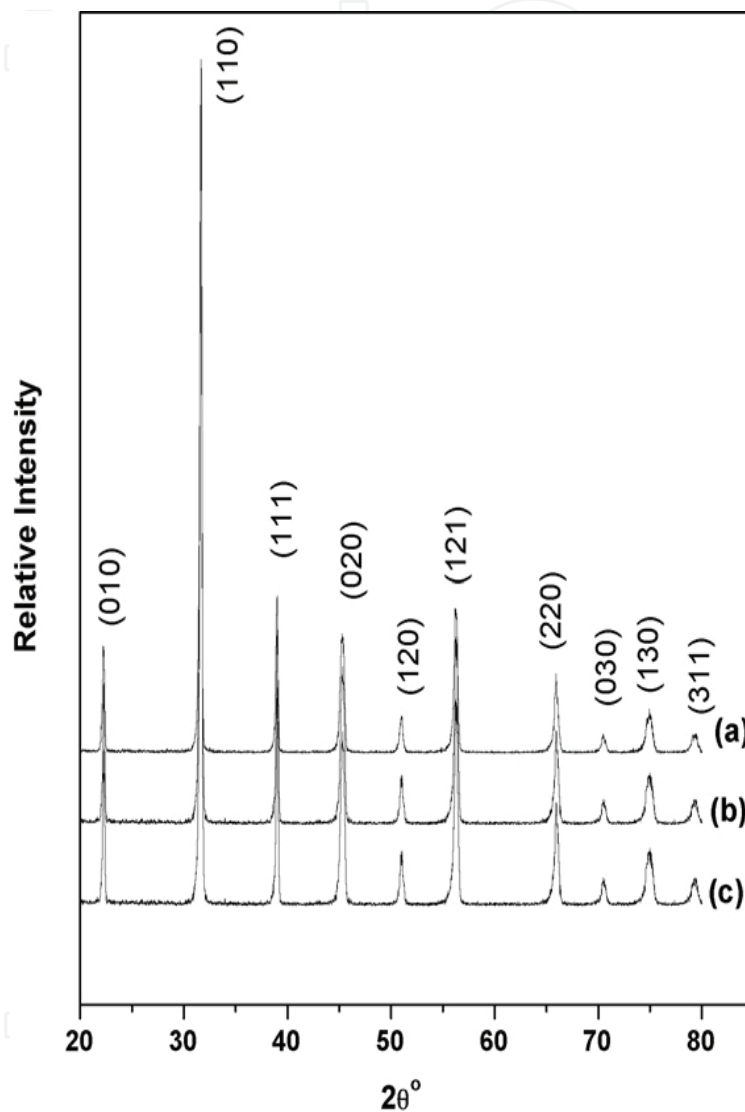

Fig. 2. X-ray diffraction pattern of the BZT powders with different concentrations calcinated at 1200 ℃ for 2 h: (a) $Ba(Ti_{0.95}Zr_{0.05})O_3$; (b) $Ba(Ti_{0.9}Zr_{0.10})O_3$ and (c) $Ba(Ti_{0.85}Zr_{0.15})O_3$.

The linear shrinkage rate $(d(l/l_0)/dT)$ as a function of temperature for different Zr/Ti ratio are shown in Figure 3. It is noted that the sintering process is strongly influenced by Zr/Ti ratio leading to a reduction in the densification temperature. The maximum shrinkage rate occurred around 1410 °C for the composition $Ba(Ti_{0.95}Zr_{0.05})O_3$. Meanwhile, a reduction in the maximum shrinkage rate was observed for the $Ba(Ti_{0.85}Zr_{0.15})O_3$ composition, probably due to the segregation of ZrO_2 at the grain boundaries. The peak close to 980 °C indicates the sintering process intra and inter-agglomerates as a consequence of different surface area of the raw powders [ZrO_2 (5.67 m^2/g), $BaCO_3$ (1.35 m^2/g) and TiO_2 (53.71 m^2/g)].

Considering the results of linear shrinkage rate, new samples were obtained from powders calcined at 1200 °C and sintered in static air at 1550 °C for 4 hours in the tubular furnace.
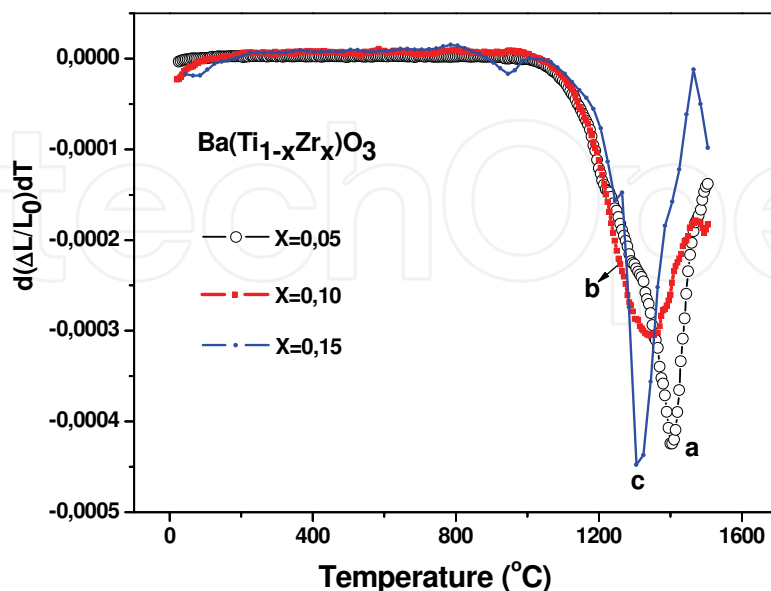

Fig. 3. Linear shrinkage rate as a function of temperature for BZT powders calcinated at 1200 °C for 2 h in different concentrations: (a) $Ba(Ti_{0.95}Zr_{0.05})O_3$; (b) $Ba(Ti_{0.9}Zr_{0.10})O_3$ and (c) $Ba(Ti_{0.85}Zr_{0.15})O_3$.

The Raman Spectra from these samples were presented in Figure 4. The directions of the phonon wave vectors are randomly distributed from one grain to another with respect to the crystallographic axes because the grains are random oriented in the precursor powders. The evolution of Raman spectra with Zr substituting on Ti sites shows some interesting changes with increasing Zr content the Raman line at 123 cm^{-1} has not been observed. Taking the mass ratio Zr/Ti = 1.9 into consideration this mode frequency is expected to be about 129 cm^{-1} for Zr replacing Ti sites, which will be reduced further by an increase in the ionic radius [$R(Ti^{4+})$ = 0.0745 nm, $R(Zr^{4+})$ = 0.086 nm]. The additional mode could therefore be associated with a normal mode involving Zr atoms. Since this mode disappears in the $Ba(Ti_{0.9}Zr_{0.10})O_3$ and $Ba(Ti_{0.85}Zr_{0.15})O_3$ compositions, it may be considered an indication of the orthorhombic to rhombohedral phase transition. Such observations could not be observed in the X-ray studies due to the different coherence length and time scale involved in the process.

Measurements on dielectric permittivity as a function of temperature reveal anisotropic behavior, Figure 5. The highest permittivity (ε_r= 14.500) is observed for the $Ba(Ti_{0.95}Zr_{0.05})O_3$ composition at 100 kHz. Three distinct phase transitions were observed and the Curie temperature reduces with the increase of zirconium content due the changes in crystal structure, as shown in Raman spectra, Figure 4. A strong reduction in the dielectric permittivity for the $Ba(Ti_{0.85}Zr_{0.15})O_3$ system is a consequence of changing in crystal structure. A sharp phase transition is indicative of a ferroelectric-relaxor behavior as observed in the literature (Yu et al.,2000; Weber et al.,2001).

Well saturated hysteresis loops with regular shape, typical of ferroelectric materials were evident for all investigated systems (Fig. 6a–c). There is no evidence of "imprint" phenomena indicating that ceramics present few defects as oxygen vacancies which pinning
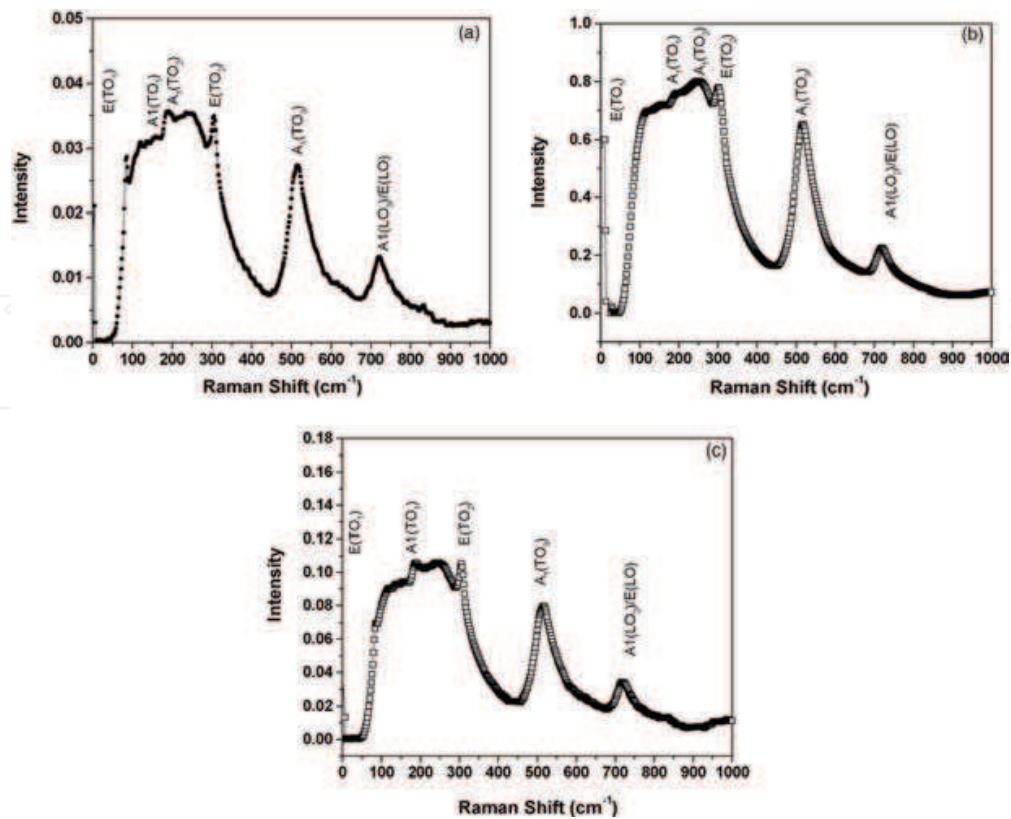
Fig. 4. Room temperature depolarized Raman spectra for BZT powders with different concentrations calcinated at 1200°C for 2h: (a) $Ba(Ti_{0.95}Zr_{0.05})O_3$; (b) $Ba(Ti_{0.9}Zr_{0.10})O_3$ and (c) $Ba(Ti_{0.85}Zr_{0.15})O_3$.

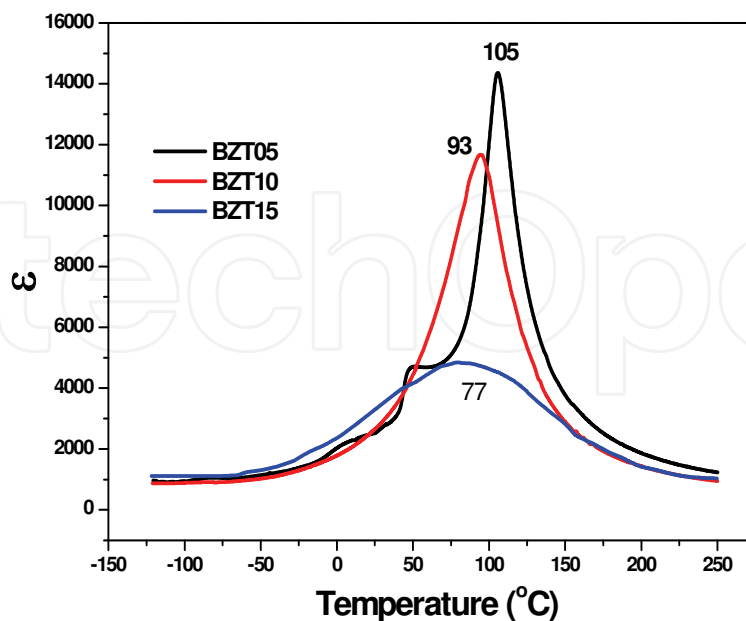Fig. 5. Temperature dependence of dielectric permittivity (ε) for BZT pellets with different concentrations, sintered at 1550 °C/4h: (a) $Ba(Ti_{0.95}Zr_{0.05})O_3$; (b) $Ba(Ti_{0.9}Zr_{0.10})O_3$ and (c) $Ba(Ti_{0.85}Zr_{0.15})O_3$.
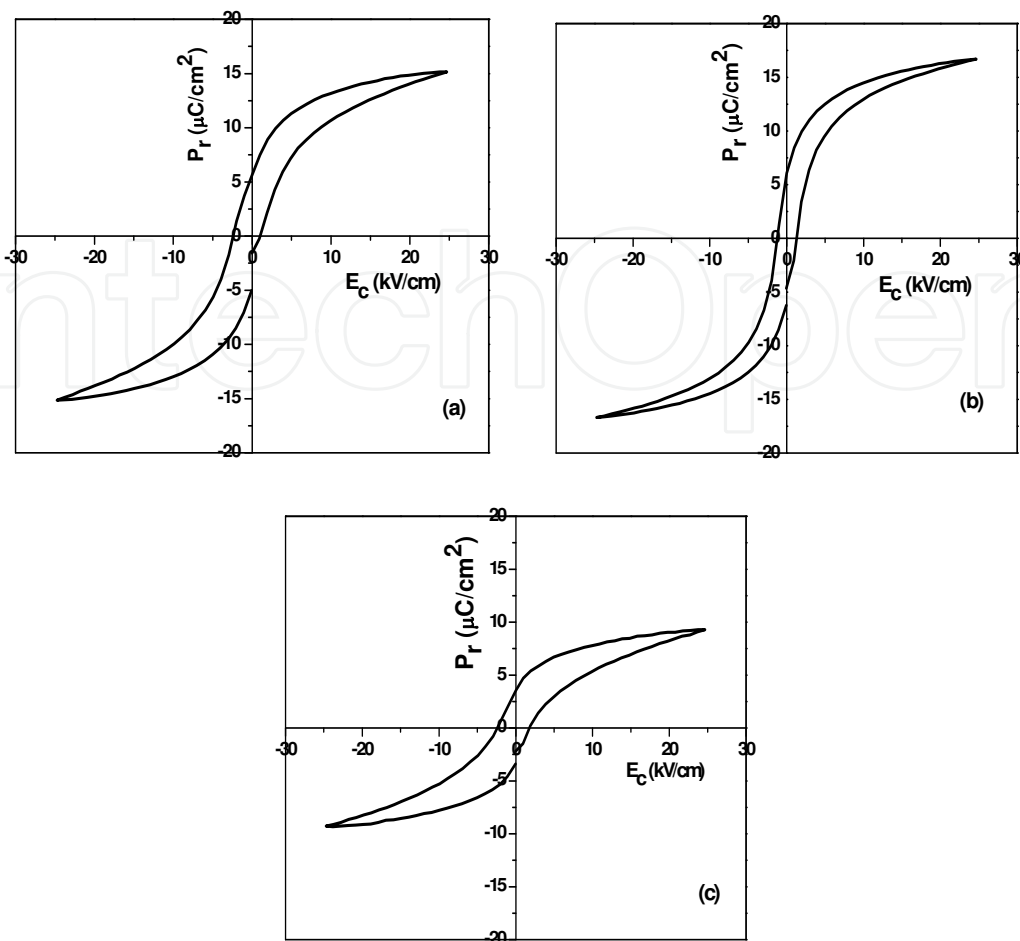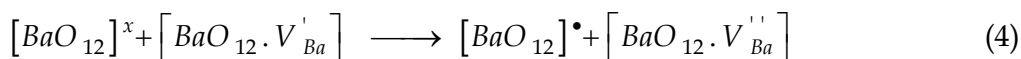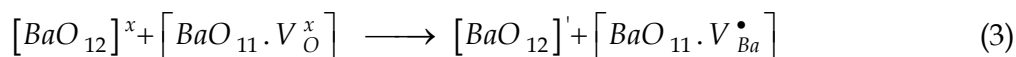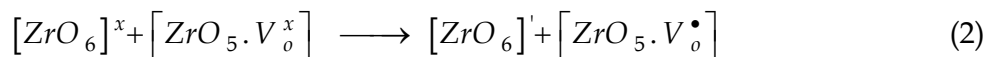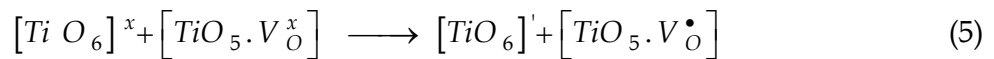
Fig. 6. P–E hysteresis loops for BZT pellets sintered at 1550 °C for 4 h in different
concentrations: (a) Ba(Ti$_{0.95}$Zr$_{0.05}$)O$_3$; (b) Ba(Ti$_{0.9}$Zr$_{0.10}$)O$_3$ and (c) Ba(Ti$_{0.85}$Zr$_{0.15}$)O$_3$.

the domain walls difficulting the saturation of hysteresis loops. The reduction in the
remnant polarization for the Ba(Ti$_{0.85}$Zr$_{0.15}$)O$_3$ system can be related to changes in crystal
structure which can explain the relaxor behavior observed in Figure 5. The defects generated
during sintering can be described by Equations 1 to 5. The substitution of Ti^{4+} for Zr^{4+}
promotes defects type $\left[TiO_5 . V_O^\bullet\right]$ that compete with the species TiO_6 raising the dielectric
and ferroelectric properties of ceramics a maximum value when compared to
species $\left[TiO_5 . V_O^\bullet\right]$ that are much smaller than $\left[TiO_6\right]$.

$$ZrO_2 \xrightarrow{BaTiO_3} Zr_{Ti}^x + 2O_O^x \tag{1}$$

$$\left[ZrO_6\right]^x + \left[ZrO_5 . V_o^x\right] \longrightarrow \left[ZrO_6\right]' + \left[ZrO_5 . V_o^\bullet\right] \tag{2}$$

$$\left[BaO_{12}\right]^x + \left[BaO_{11} . V_O^x\right] \longrightarrow \left[BaO_{12}\right]' + \left[BaO_{11} . V_{Ba}^\bullet\right] \tag{3}$$

$$\left[BaO_{12}\right]^x + \left[BaO_{12} . V_{Ba}'\right] \longrightarrow \left[BaO_{12}\right]^\bullet + \left[BaO_{12} . V_{Ba}''\right] \tag{4}$$

$$\left[Ti\, O_6 \right]^{x} + \left[TiO_5 . V_O^{x} \right] \longrightarrow \left[TiO_6 \right]' + \left[TiO_5 . V_O^{\bullet} \right] \tag{5}$$

3. Temperature dependence and Dielectric response of tungsten or vanadium modified Ba(Ti$_{0.90}$Zr$_{0.10}$)O$_3$ ceramics

3.1 Sample preparation of tungsten or vanadium modified Ba(Ti$_{0.90}$Zr$_{0.10}$)O$_3$

As observed, BZT phase presents interesting behavior that need to be exploited. A much discussed variable is the influence of donor elements (W^{6+} or V^{5+}) whose effects depend on concentration and processing of the powder. The main motivation for using V^{5+} or W^{6+} as network modifier was the possibility of obtaining ceramics with high dielectric constant and shifted the phase transition to lower temperatures, in the range of 70 to 120°C. Move the sintering temperature to less than 1550°C used for ceramics Ba(Ti$_{1-x}$Zr$_x$)O$_3$, was also a goal to be achieved. The Ba(Ti$_{0.9}$Zr$_{0.10}$)O$_3$ composition was chosen because among those studied showed a single phase transition Figure 5. In this study Ba(Zr$_{0.10}$Ti$_{0.90}$)O$_3$ powders were prepared by mixed oxide method as described in the item 2.2. Temperature dependence and Dielectric response from vanadium modified Ba(Ti$_{0.90}$Zr$_{0.10}$)O$_3$ ceramics

According to X-ray diffraction analysis the single phase crystallized in a perovskite structure were obtained. The X-ray diffraction patterns for the pure BZT and doped with different concentrations of vanadium sintered at 1350°C show a pure phase for concentrations up to 2mol % of dopant. On the other hand, when the vanadium content increases to (3-6 mol %) an intermediate phase of BaV$_2$O$_6$ has been obtained, Figure 7(a). Also, small traces of unreacted oxides such as TiO$_2$ and ZrO$_2$ are located at 2θ = 27 and 46 degree for the pure BZT:10 phase. Bragg reflection peaks are indicative of perovskite structure, mainly characterized by higher intense peak (110) at 2θ = 31° and no apparent peak splitting is identified. This is a indication that the addition of vanadium up to 2wt% has formed a stable solid solution in the BZT matrix lattice at 1350°C. The X-ray diffraction pattern Figure 7(b) obtained from the BZT:2V ceramics sintered at various temperatures show that the single phase with a tetragonal perovskite structure with highest intensity peak at 31° was obtained. At low temperature (1200°C) although diffraction peaks corresponding to the tetragonal perovskite structure they are generally weak indicating a poor crystallinity of the ceramics in the (1 1 0) and (2 2 0) directions. At 1350°C the growth of (110) and (220) oriented grains was noted.

Raman spectrum located at 915 cm^{-1} indicates the presence of vanadium in the BZT structure as observed through X-ray diffraction. The substitution located in B site of perovskite BZT-10 reduces the distortion of the octahedral sites leading to a more organized symmetry when increasing the concentration of vanadium ions.

The degree of order-disorder of the atomic structure was observed by Raman spectroscopy in the longitudinal (LO) and transverse (TO) modes, Figure 8. These modes are associated with electrostatic and ionic forces from structure due to Ba^{2+} in BaTiO$_3$ (Domenico Jr et al.,1968; Chaves,et al.,1974) . For the perovskite Ba(Zr$_{0.10}$Ti$_{0.90}$)O$_3$, Ba^{2+} ions are illustrated by bands on the spectra, A1 (TO1) and A1 (TO2) around 193 and 517 cm^{-1} (Dobal et al.,2001; Kreiselet al., 2004). The other modes OE1 (TO1) and E1 (TO2) located at 116 and 301 cm^{-1} are associated to tetragonal - cubic transition, whereas the A1 (LO3) mode was found at 720 cm^{-1} due the zirconium replacing titanium in B site. However, the coupling between the A1 (TO1) and A1 (TO2) modes reduces the intensity of A1 (TO2) mode (Dobal et al.,2001; Dixit et al.,2004).
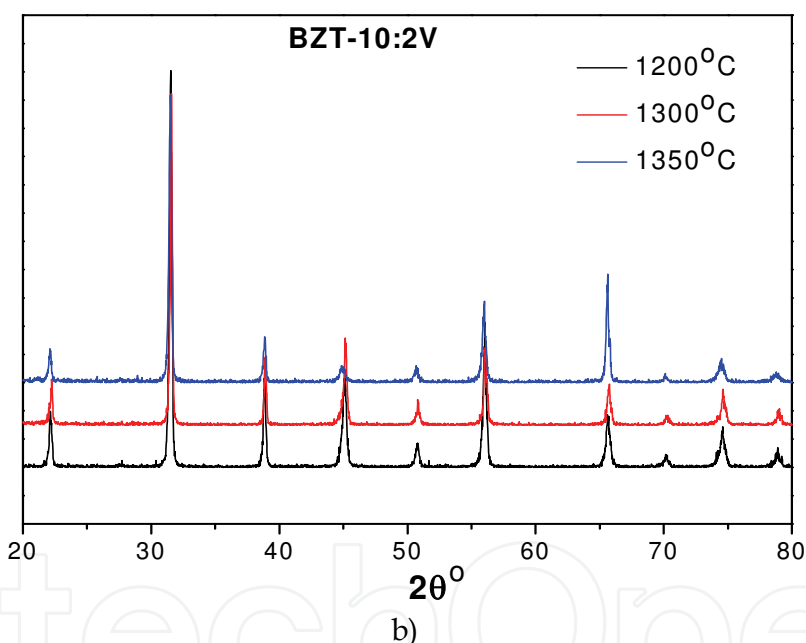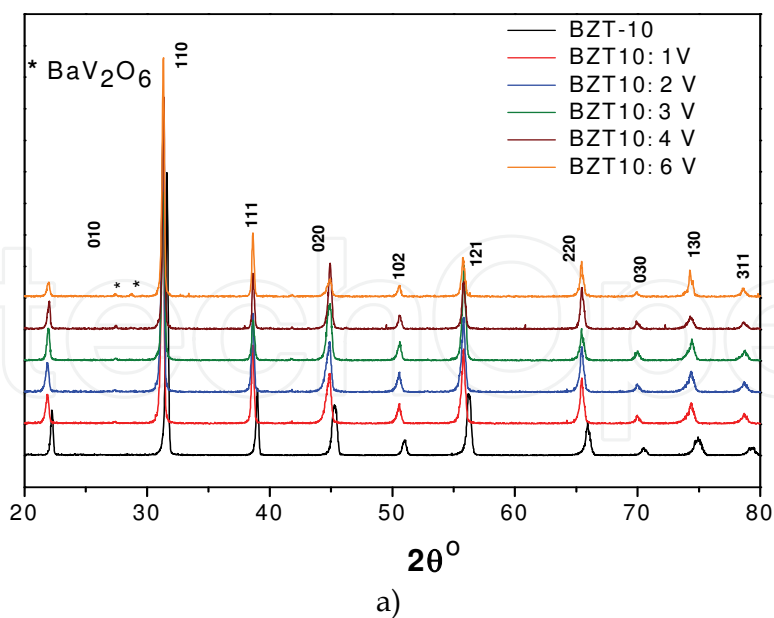
Fig. 7. X-ray diffraction of BZT10 and BZT10:xV ceramics sintered : (a) at 1350 °C for 4 hours; (b) BZT10:2V ceramics sintered at diferentes temperatures.

The temperature dependence of dielectric permittivity for BZT:2V samples at 10 kHz is shown in Figure 9a. For coarse-grained sample (1350°C) the phase transition is observed at 92°C with maximum dielectric permittivity (ε_m) 15.000. In this sample, it was noted a structural phase transition which corresponds to the paraelectric (cubic) to ferroelectric (tetragonal) phase transition at Tc. For medium and small-grained samples only one phase transition is observed. However, the peak associated to phase transition temperature for the small-grained sample become broader than that of the big and medium grain size. These results suggest that the BZT ceramics with small grain size has the transition from a normal ferroelectric to 'relaxor-like' ferroelectric (Zhi, et al.,2002). The dielectric permittivity

increases gradually with an increase at temperature up to the transition temperature (Tc) and then decreases. This increasing is caused by the relatively large ionic radius of the B ion which enhances the thermal stability of the BO_6 octahedra when compared to Ti^{4+} or Zr^{4+}.

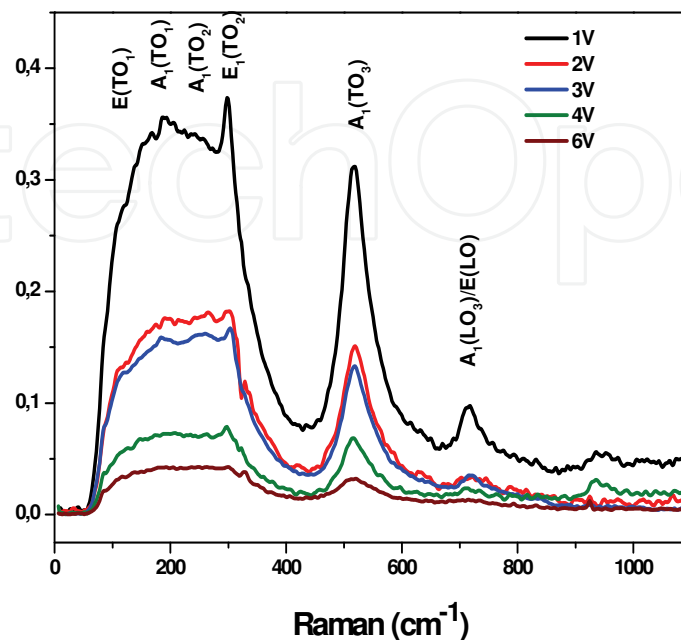Fig. 8. Room temperature depolarized Raman spectra for BZT10:xV powders calcinated at 1200°C for 2hours

Also, the packing density of the BO_6 octahedra will be determined by the size of the B ion. Larger B ions give more closely packed octahedral which are therefore more stable. The V^{5+} enters in the B-site of the ABO_3 perovskite lattice leading to a charged [VO6]• defect which is associated with a barium vacancy in a local barium cluster [$V''_{Ba} O_{12}$]. In fully or partly ionic compounds vacancies are charge balanced by other defects forming an overall neutral system. It can be assumed that particle charge compensation takes place at a nearest-neighbor barium cluster site in the [BaO_{12}], because the resulting coulomb interaction is the most important driving force. This assignment is in accordance with first-principles calculation (Anicete-Santos et Al., 2005). Probably, an equilibrium can be reached between "free" [VO6]• centers and [VO6]• + [$V''_{Ba} O_{12}$] associated defects. We can consider the free [VO6]• clusters as responsible for ionic mobility and [VO6]• + [$V''_{Ba} O_{12}$] defect dipole complexes the main cause of electrical properties in the ceramic. Hence, charge transport will be considerably hindered. Below the Curie temperature, a high dependence of dielectric loss was observed while at elevated temperatures, vanadium doping stabilizes this dependence, Figure 9b. The possible formation of dipole complexes may result in a reduced dielectric loss at elevated temperatures. This reflects that good insulation resistance was maintained at high temperatures, which is important for high temperature piezoelectric applications. The dielectric loss shows strong dependence as temperature increases. At the same frequency region, the obtained values are 0.001 (1200°C) to 0.019 (1300 and 1350 °C). It is known that the increase of dissipation factor is due to extrinsic resonance behavior (Veith et al., 2000) This may be due to the defects (vacancy, movable ion, leaky grain boundary

(Hoffmann & Waser, 1997) that developed in the structure of the bulk material with the increase of sintering temperature. The sample sintered at low temperature possesses a significant difference in the dielectric loss peak suggesting a pinch-off of phase transition. In this sample, due the fine-grain microstructure the introduction of vanadium causes a more sensitive distortion of the perovskite lattice leading to a reduction in the oxygen octahedron interstices. The distortion of the perovskite lattice can strengthen the structure fluctuation of the BZT:2V ceramics which can be account for different behavior of diffusion phase transition characteristics in this sample. [ZrO6]x, [TiO6]x, and [VO6]• clusters are present in the BZT:2V lattice. As the temperature increases, there is a charge transference of [VO6]• to the Ti and Zr clusters, according to Equations (6) and (7):

$$[VO6]• + [ZrO6]x \rightarrow [VO6]x + [ZrO6]• \tag{6}$$

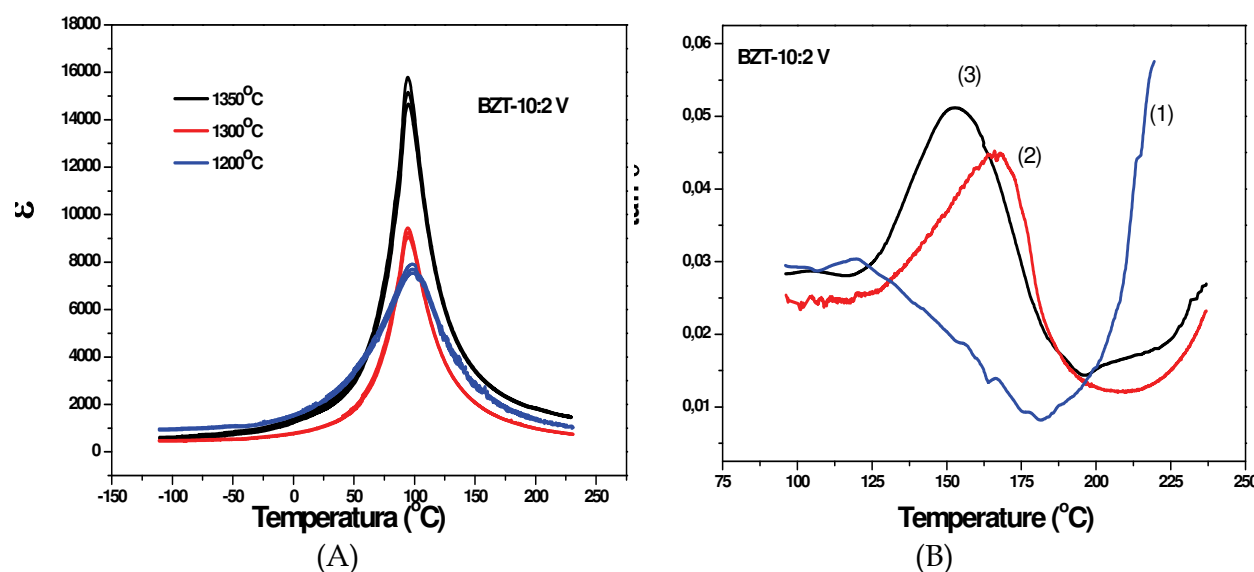$$[VO6]• + [TiO6]x \rightarrow [VO6]x + [TiO6]• \tag{7}$$

Fig. 9. Temperature dependence of dielectric permittivity (A); and dielectric loss (B) at 10 kHz for BZT10:2V ceramics sintered at (1) 1200, (2) 1300 and (3) 1350 °C for 4 hours.

Scanning electron microscopy of vanadium doped BZT10 with different concentrations shows that there is formation of a liquid phase at the grain boundary with increasing concentration of vanadium, figure 10 (a) to (c). Scanning electron microscopy also allowed to observe the behavior of the sample BZT10:2V sintered at 1200 C, 1300°C and 1350°C where the increase in temperature promoted the diffusion of vanadium with the formation of defects that are represented in equations 6 and 7. These phenomena promote the grain growth and improves the dielectric permittivity.

4. Temperature dependence and dielectric response from tungsten modified Ba(Ti$_{0.90}$Zr$_{0.10}$)O$_3$ ceramics

XRD patterns of BZT and BZT10:yW modified ceramics are shown in Figure11. Small traces of unreacted oxides such as TiO$_2$ and ZrO$_2$ are located at 2θ = 27 and 46 degree for the

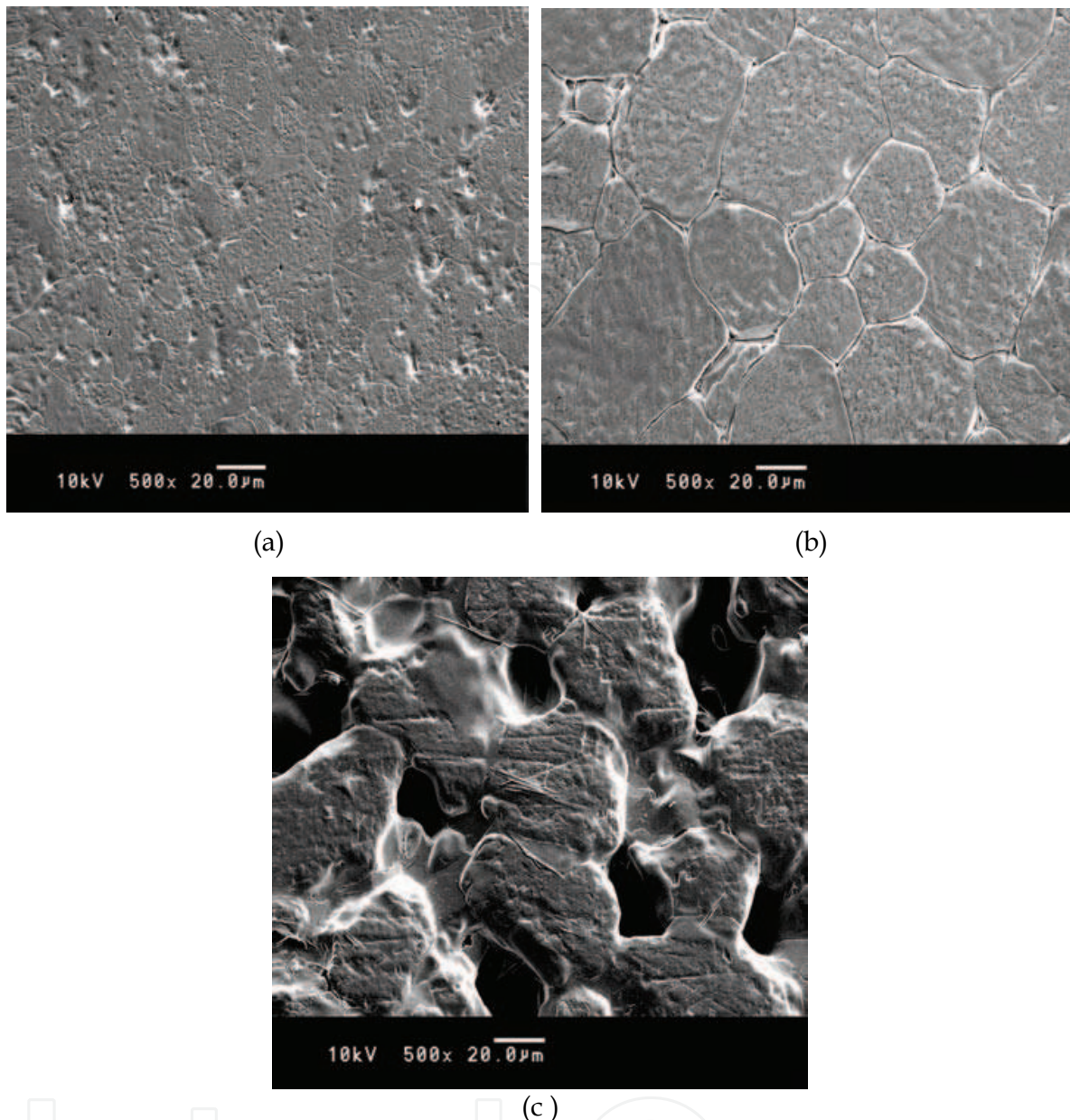(a)   (b)

(c)

Fig. 10. SEM photomicrographs of the polished surface of BZT-10 ceramic modified with vanadium ions and sintered at 1350°C for 4 h, (a) BZT10:1V; (b) BZT10:2V; (c) BZT10:6V

BZT10 phase. On the other hand, no secondary phases are evident in the BZT10:1W and BZT10:2W powders. This is a clear indication that the addition of tungsten is forming a stable solid solution in the *BZT* matrix lattice. As tungsten content increases, there was an intermediate phase of $BaWO_3$ was obtained. Bragg reflections peaks are indicative of perovskite structure, mainly characterized by higher intense peak (hkl-110) at $2\theta = 31°$ and no apparent peak splitting is identified.

The evolution of Raman spectra in the tungsten substituted BZT ceramics displayed in Figure 12 shows some interesting order-disorder degree of the atomic structure at short range. The spectrum presents the stretching mode of A1(TO1) and A1(TO3) at around 193 and 517 cm⁻¹. The E1(TO1) and E1(TO2) modes that have been associated with the tetragonal-cubic phase transition were observed at 116 and 301 cm⁻¹. Whereas the A1(LO3)
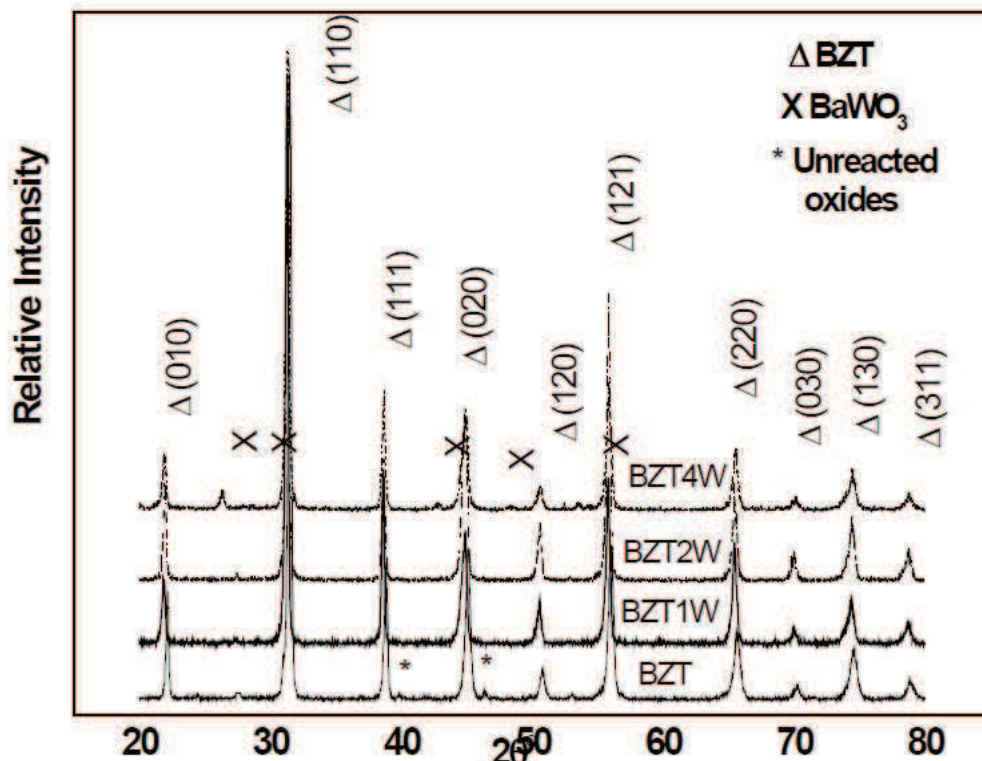
Fig. 11. X-ray diffraction for BZT10, BZT10:1W, BZT10:2W and BZT10:4W powders prepared from mixed oxide method, calcined at 900°C for 2 hours.
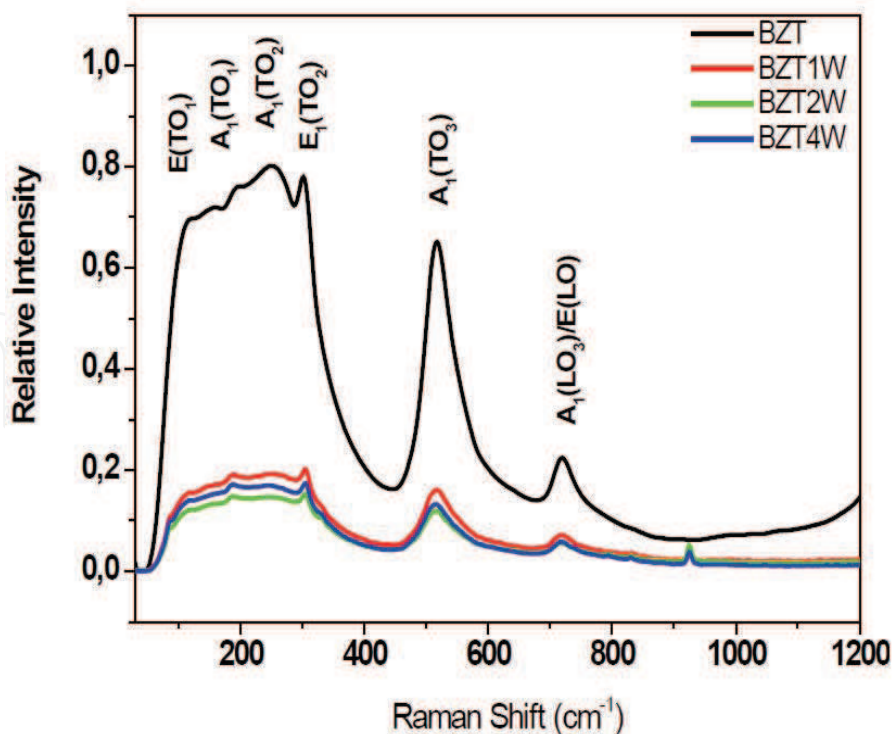

Fig. 12. Room temperature depolarized Raman spectra for BZT10, BZT10:1W, BZT10:2W and BZT10:4W powders prepared from mixed oxide method, calcined at 900°C for 2 hours.

mode was found at 720 cm^{-1} with zirconium (Zr) substituting on titanium (Ti) sites, as tungsten is incorporated in the BZT lattice, a Raman line at 925 cm^{-1} appears. Considering that tungsten substitutes the B-site of the lattice, as its content increases the relative intensity of bands reduces due to the distortion of octahedral sites. This results in diminished interstices in oxygen octahedron. Such observations could not be observed in the X-ray studies due to the different coherence length and time scale involved in the process.

The microstructure of those ceramics is shown in Figure 13. The grain growth is inhibited in the BZT10:4W sample due to the formation of BaWO$_3$ secondary phase in the grain boundary, Figure 13 d. Tungsten ion plays a role of donor in BZT because it possesses a higher valence than Ti or Zr ions suppressing the formation of oxygen vacancies. Considering that W^{+6} preferentially enter in B-sites, we expected an increase in oxygen vacancies concentration which affects the densification process. The small grain size can be interpreted by the suppression of oxygen vacancy concentration, which results in slower oxygen ion motion and lower grain growth rate as it was verified in the EPR spectra. No segregates in the grain boundaries of the BZT10:2W sample indicates the high solubility of WO$_3$ in the BZT matrix (Figure 13 c).

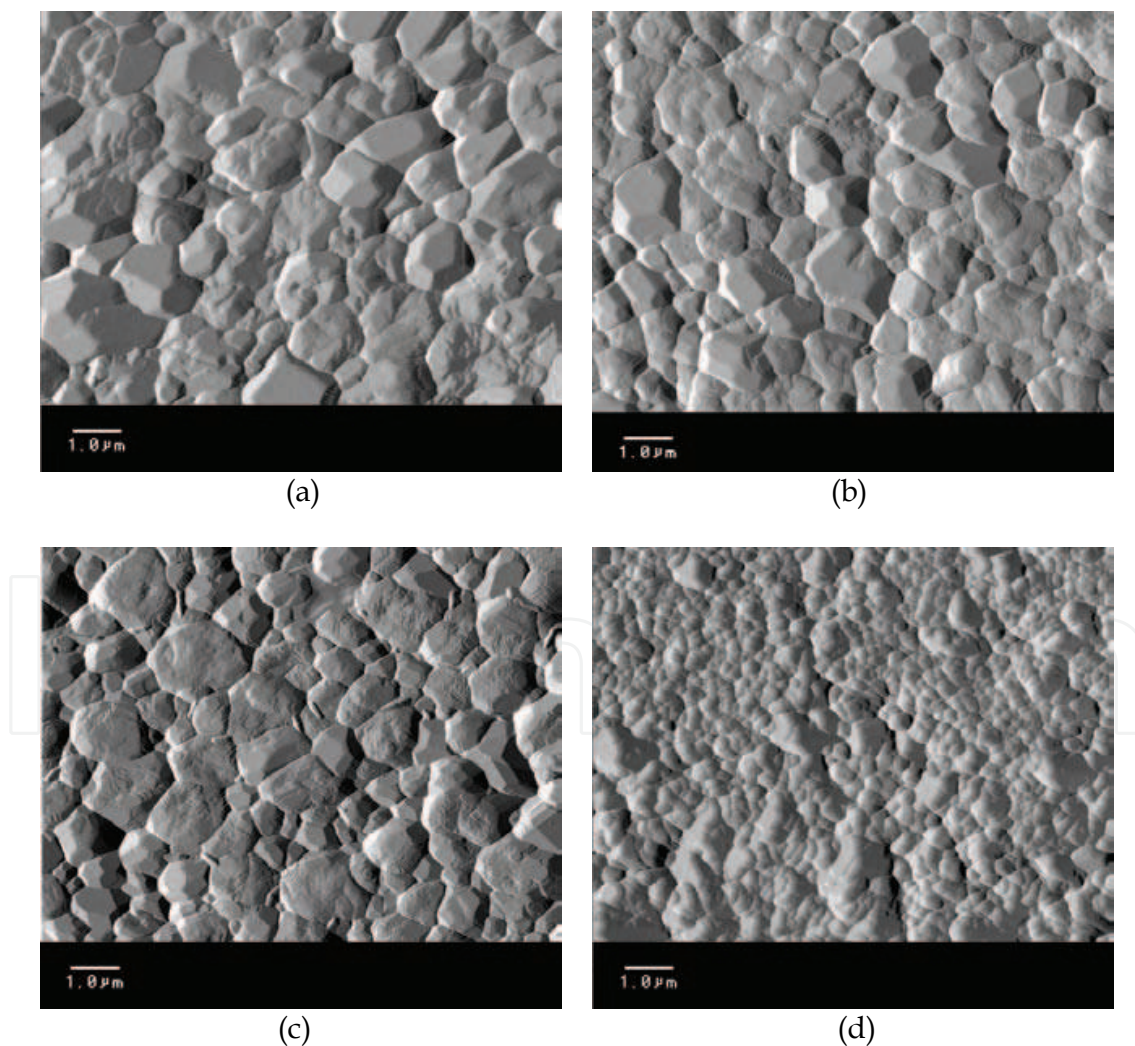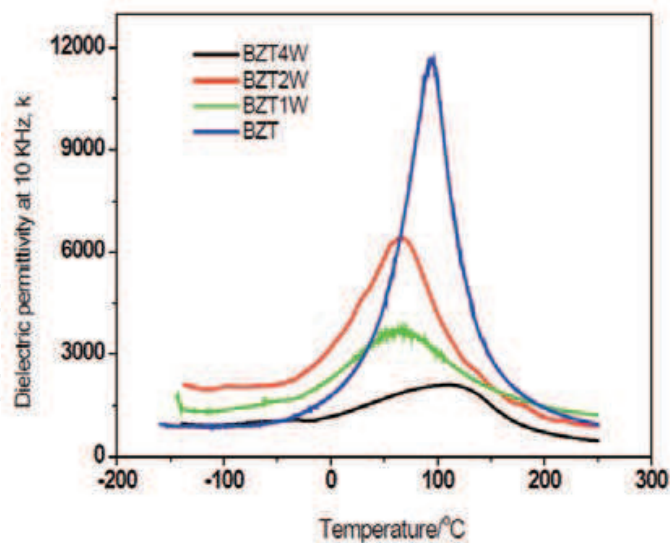Fig. 13. Micrographies for (a) BZT10, (b) BZT10:1W, (c) BZT10:2W and (d) BZT10:4W ceramics prepared from mixed oxide method , sintered at 1200°C for 4 hours.
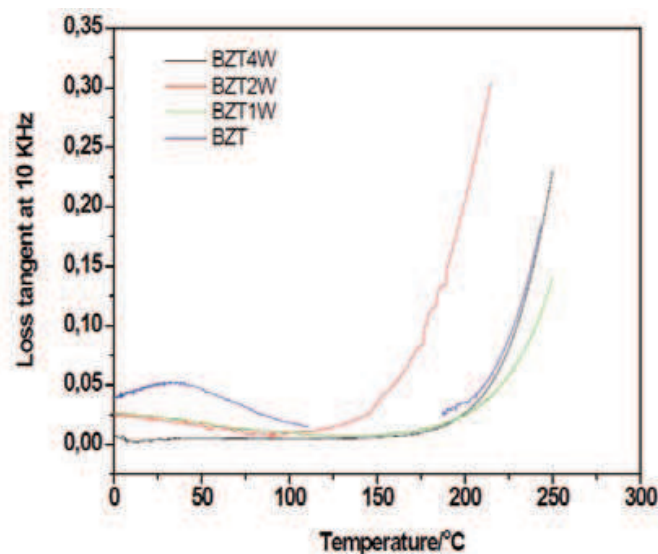
The temperature dependence of relative dielectric permittivity and dielectric losses measured at 10 KHz for selected BZT compositions are show in Figure 14. Substitution of W^{6+} in the B-site will lead to the distortion of the perovskite lattice leading to reduction of phase transition temperature up to tungsten content of 2 wt.% and broadening of dielectric peak. Since the ionic radius of W^{6+} is smaller (0.62Å) than that of Ti^{4+} (0.68Å) on B-site, increasing its amount would lead to a reduced contribution of overall atomic polarization. The dielectric permittivity increases gradually with an increase in temperature up to the transition temperature (T_c), Curie point, and then decreases. The region around the dielectric peak is broadened due to a disorder in the cations arrangement in one or more crystallographic sites of the structure (Lines & Glasss,1977; Wu et al.,2002). Large differences in the B valence results in a strong tendency for the material to disorder in one or more crystallographic sites leading to a microscopic heterogeneity in compounds with different Curie points. According to Wu et al.,2002 the dielectric permittivity consists of contributions of ionic and atomic polarization only. Therefore, the increase of dielectric permittivity may be attributable to increased ionic polarization. (Jin et al. 2001) proposed that the phase transition is caused by instability of the BO_6 octahedra. The relatively larger ionic radius of the B ion enhances the thermal stability of the BO_6 octahedra, when compared to Ti or Zr ions (Wu et al.,1983). This results in an increase of BO_6 volume octahedron and consequently decreasing its stability which results in a reduction of phase transition that involves structural inhomogeneity and existence of polar nanoregions. The interstices in oxygen octahedron will be diminished with the increase of metal vacancies in the B-site, and the c/a ratio will be lowered as well. Therefore, the dielectric polarization is depressed owing to the restraint of the B-site cations, and as a result the Curie point will lead to a diffuse phase transition. The dielectric permittivity is reduced with the increase in tungsten content leading to a typical relaxor behaviour, Figure 14a. At lower temperatures, a small dependence of dielectric loss was observed while at elevated ones, there is a significant dependence on it. Also, a small peak just below T_c was evident in the BZT, Figure 14b. It should be pointed out that this behaviour can be explained by the appearance of polar microregions in the samples. The dielectric relaxation peak can be attributed to the electron-relaxation-mode coupling mechanism in which carriers (or polarons, protons, and so on) are coupled with existing dielectric modes suggesting that the motion of carriers (or polaron hopping) is responsible for this behavior (Xu,1991). Poor insulation resistance was maintained at high temperatures indicating that these ceramics can be used for low temperature capacitor applications. In addition, the dielectric loss was much lower than that of the undoped BZT reported in our previous work (Wu et al.,1983; Moura et al.,2009; Moura et al.,2010; Marques et al., 2007) which is attributed to the decrease in space charge density as tungsten was incorporated in the BZT lattice. Two main mechanisms can be considered for substituting W^{+6} for Ti^{+4} in the BZT lattice. The compensation mechanism for substituting a ion^{6+} for a ion $^{4+}$ should reduce the oxygen vacancy concentration, leading to formation of Ba^{2+} vacancies. Another possibility is that the extra electrons become somewhat delocalized leading to some conductivity.

EPR Hamiltonian parameters were used to perfectly reproduce the observed sequence of symmetrical peak pattern of the fine structure, Figure 15. The substitution of W^{6+} in the Ti^{4+} site (Figure15b) causes a slight distortion in the spectra increasing disorder and symmetry changes in the BZT lattice (Figure 15a).

BZT10:2W spectra shows hyperfine bands typical for materials with spin 5/2 which can be attributed to the Zr presence as proposed in Figure 15b. (Abraham,et al.,1986). Moreover,

(A)

(B)

Fig. 14. Temperature dependence of dielectric permittivity (A); loss tangent (B) mesured at 10 KHz for BZT10, BZT10:1W, BZT10:2W, BZT10:4W ceramics prepared from mixed oxide method sintered at 1200°C for 4hours.

it suggests almost isotropic neighbourhood of the isolated Zr and Ti ions in the pattern. The obtained signal is typical for single ionized oxygen vacancies VO(, as observed by (Zhang et al.2004). The hyperfine bands in the spectra correspond to the expected line broadening attributed to dipolar interactions of tungsten in the host, according to reaction of defects as discussed in literature (Shannigrahi et al., 1999). Substitution of Ti^{4+} by W^{6+} causes distortion in the crystal structure changing lattice parameter. In this structure, $[TiO5.Vox]c$ clusters are donor candidates and $[TiO_6]$ xc are acceptors candidates. $[TiO_5.Vo^x]c$ have shown two paired electrons $\underline{\uparrow\downarrow}$, $[TiO_5.Vo^x]c$ have shown one unpaired electron, while $[TiO_5.Vo^x]c$ have shown no unpaired electrons. The source of hyperfine bands can be a result of interaction between an ion with unpaired electrons with species which present complex vacancies. This is supported by the high symmetry as inferred from Raman studies. The main differences in

the spectra correspond to the expected line broadening attributed to dipolar interactions of tungsten in the host according to equations 8 -15.
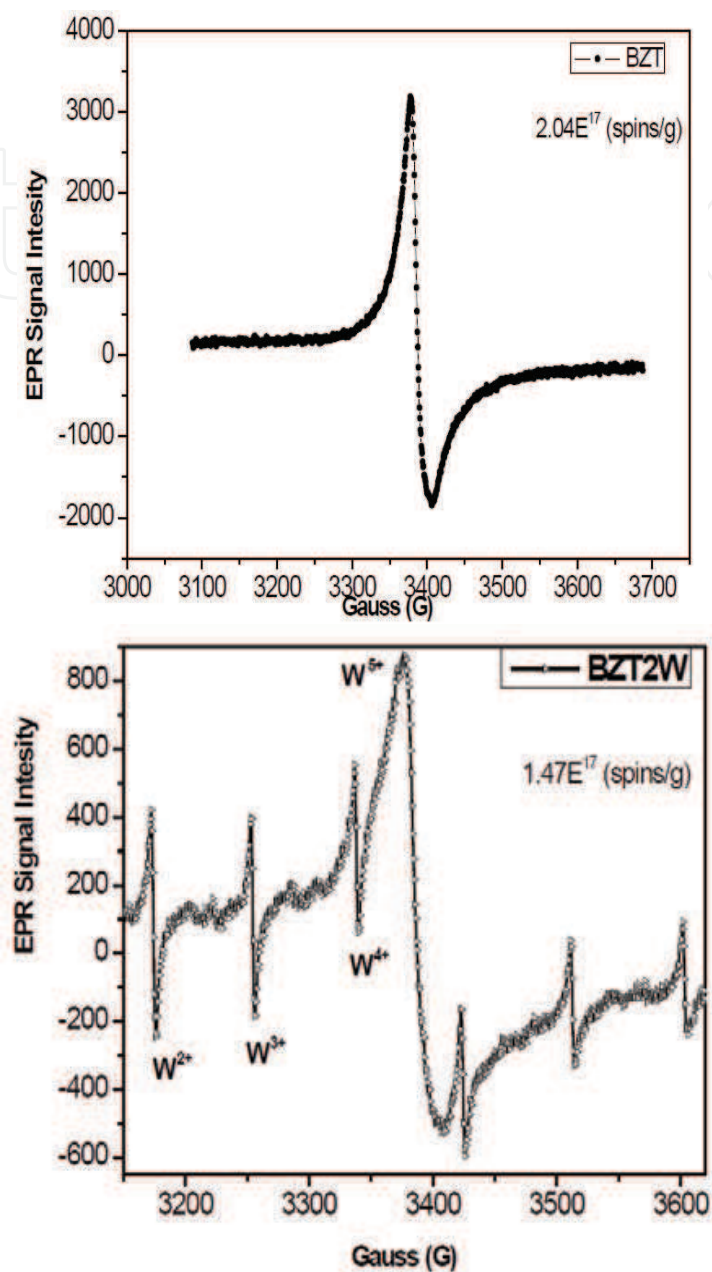
Fig. 15. Electron paramagnetic resonance measurements for BZT10 and BZT10:2W powders prepared from mixed oxide method, calcined at 900°C for 2 hours.

The corresponding defect reactions can be described as follows:

$$WO_3 \xrightarrow{BZT} W_{Ti}^{\bullet\bullet} + V_{Ba}'' + 3\,O_O^x \tag{8}$$

$$[MO_6]^{x+} \longrightarrow [MO_6]' + [MO_5 . V_o^{\bullet}] \tag{9}$$

For M = Zr or Ti

$$\left[V \, {}_{Ba}'' \, O \, {}_{12} \right] + \left[WO_6 \right]^{\bullet\bullet} \longrightarrow \left[V \, {}_{Ba}^{x} \, O \, {}_{12} \right] + \left[W O_6 \right]^{x} \tag{10}$$

$$\left[MO \, {}_5 \, V \, {}_O^{x} \right] + \left[WO_6 \right]^{\bullet\bullet} \longrightarrow \left[M O \, {}_5 \, V \, {}_O^{\bullet} \right] + \left[WO_6 \right]^{\bullet} \tag{11}$$

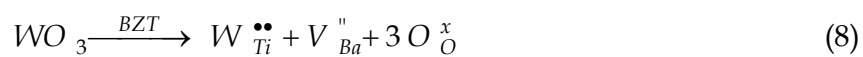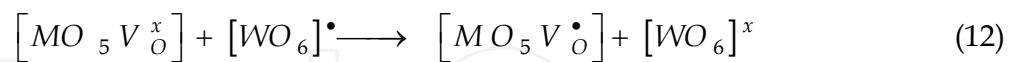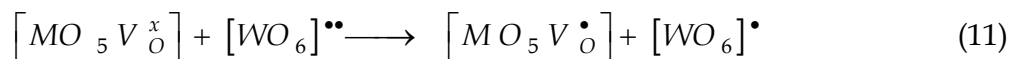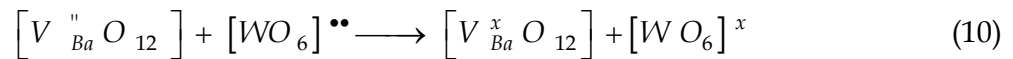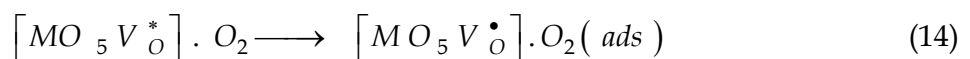$$\left[MO \, {}_5 \, V \, {}_O^{x} \right] + \left[WO_6 \right]^{\bullet} \longrightarrow \left[M O \, {}_5 \, V \, {}_O^{\bullet} \right] + \left[WO_6 \right]^{x} \tag{12}$$

$$2 \left[MO \, {}_6 \right]' + \left[WO_6 \right]^{\bullet\bullet} \longrightarrow 2 \left[WO_6 \right]^{x} + \left[WO_6 \right]^{x} \tag{13}$$

Despolarization of $\left[MO \, {}_6 \right]^{x}$ clusters

$$\left[MO \, {}_5 \, V \, {}_O^{*} \right] . \, O_2 \longrightarrow \left[M O \, {}_5 \, V \, {}_O^{\bullet} \right] . O_2 \left(ads \right) \tag{14}$$

$$\left[MO \, {}_5 \, V \, {}_O^{*} \right] . O_2 \longrightarrow \left[M O \, {}_5 \, V \, {}_O^{\bullet\bullet} \right] . O \, {}_2' \tag{15}$$

High $\left[V \, {}_O^{\bullet} \right]$ concentration adsorbs O_2 leading to $\left[M O \, {}_5 \, V \, {}_O^{\bullet\bullet} \right] . O \, {}_2'$ species.

Increasing tungsten concentration leads to $[MO_5V_O^{\bullet\bullet}] \cdot O_2'$ clusters. This species favour the creation of oxygen vacancies in $[TiO_6]$ or $[ZrO_6]$ sites, most of that being considered as complex vacancies in order-disorder structure. As a consequence, the oxygen vacancy-acceptor ion dipole may interact with polarization within a domain making its movement more difficult to switch. Ferroelectric hysteresis loop showed that the P_r and E_c were 3.0 $\mu C/cm^2$ and 1.25 kV/cm, respectively, Figure 16. The *P-E* loop was actually not closed
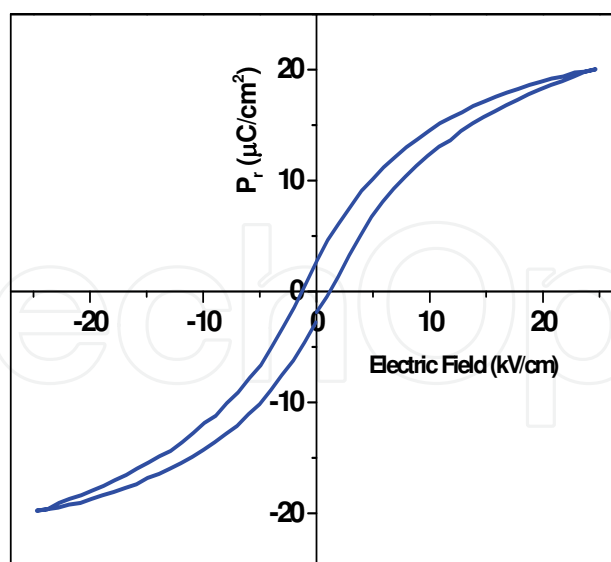

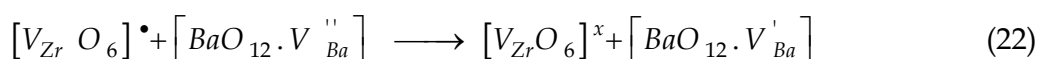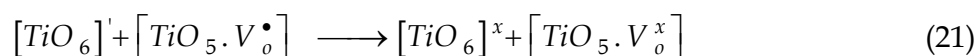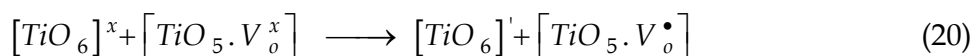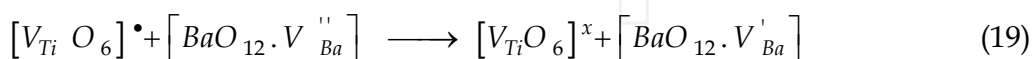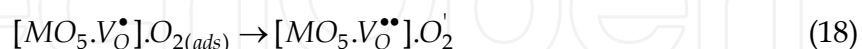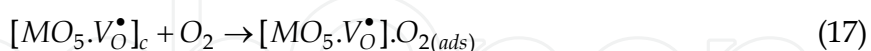Fig. 16. Hysteresis loops for BZT10:2W ceramics sintered at 1200ºC for 2 hours in a conventional furnace.

because the applied field was very high, up to 25.0 kV/cm. The obtained values pointed to the regular microstructure of the sintered specimen with small grains. The non saturation of

the hysteresis loop can be resulted from the leakage current at high electric field. In this way, the charge compensation required by addition of W[6+] ions could be achieved by reducing oxygen vacancies which induces changes in the leakage current. It also can be observed that the BZT10:2W ceramics is free of imprint phenomena which causes a shift in the coercitive field axis that leads to a failure in the capacitor. This failure can be caused by the defects as oxygen vacancies and space charges that leads to domain pinning and is almost absent in the BZT10:2W sample.

5. Influence of atmosphere on Dielectric response of vanadium modified Ba(Ti$_{0.90}$Zr$_{0.10}$)O$_3$ ceramics

Having in mind that the substitution of vanadium on B-site broads the dielectric permittivity curves due the repulsion with their next nearest neighbors leading to a structure which is tetragonally distorted and improved ferroelectric response, we have examined the effects of annealing atmospheres (oxygen, air and nitrogen) on the electrical properties of BZT:2V ceramics. The dielectric permittivity for BZT10:2V the ceramics sintered at 1350°C in nitrogen showed higher values as compared to the ceramics sintered in air and oxygen atmospheres Figure 17. Regarding dielectric loss, the measurements suggest that low frequency loss values are significantly higher in nitrogen atmosphere. This can be explained by the higher space charge concentration, again arising due to higher oxygen vacancy concentration. Another observation that can be made is that dielectric properties (both dielectric permittivity and loss tangent) of oxygen and air do not improve appreciably whereas nitrogen sintered ceramics show a significant improvement in the dielectric properties. This again emphasizes the superior quality of nitrogen sintered ceramics. It is possible that this decrease in the permittivity for oxygen and air atmospheres is caused by space charge polarization which is inherently related to the nonuniform charge accumulation. The following equations (16-26) can be use to represent the dieletric permittivity dependence on sintering atmosphere.

For M = Zr ou Ti and c = complex

$$V_2O_5 \xrightarrow{Ba(Ti_{0,90}Zr_{0,10})O_3} 2V_{Ti}^{\bullet} + V_{Ba}'' + 5O_O^x \quad ou \quad 2V_{Zr}^{\bullet} + V_{Ba}'' + 5O_O^x \tag{16}$$

$$[MO_5.V_O^{\bullet}]_c + O_2 \rightarrow [MO_5.V_O^{\bullet}].O_{2(ads)} \tag{17}$$

$$[MO_5.V_O^{\bullet}].O_{2(ads)} \rightarrow [MO_5.V_O^{\bullet\bullet}].O_2' \tag{18}$$

$$\left[V_{Ti}\,O_6\right]^{\bullet} + \left[BaO_{12}.V_{Ba}''\right] \longrightarrow \left[V_{Ti}O_6\right]^x + \left[BaO_{12}.V_{Ba}'\right] \tag{19}$$

$$\left[TiO_6\right]^x + \left[TiO_5.V_o^x\right] \longrightarrow \left[TiO_6\right]' + \left[TiO_5.V_o^{\bullet}\right] \tag{20}$$

$$\left[TiO_6\right]' + \left[TiO_5.V_o^{\bullet}\right] \longrightarrow \left[TiO_6\right]^x + \left[TiO_5.V_o^x\right] \tag{21}$$

$$\left[V_{Zr}\,O_6\right]^{\bullet} + \left[BaO_{12}.V_{Ba}''\right] \longrightarrow \left[V_{Zr}O_6\right]^x + \left[BaO_{12}.V_{Ba}'\right] \tag{22}$$

$$\left[ZrO_6\right]^x + \left[ZrO_5.V_o^{\,x}\right] \longrightarrow \left[ZrO_6\right]' + \left[ZrO_5.V_o^{\,\bullet}\right] \tag{23}$$

$$\left[ZrO_6\right]' + \left[ZrO_5.V_o^{\,\bullet}\right] \longrightarrow \left[ZrO_6\right]^x + \left[ZrO_5.V_o^{\,x}\right] \tag{24}$$

$$\left[MO_6\right]c^x + \left[MO_5.V_o^{\,x}\right]c \longrightarrow \left[MO_6\right]c' + \left[MO_5.V_o^{\,\bullet}\right] \tag{25}$$

$$\left[MO_6\right]c^x + \left[MO_5.V_o^{\,x}\right]c \longrightarrow \left[MO_6\right]c' + \left[MO_5.V_o^{\,\bullet}\right]c \tag{26}$$
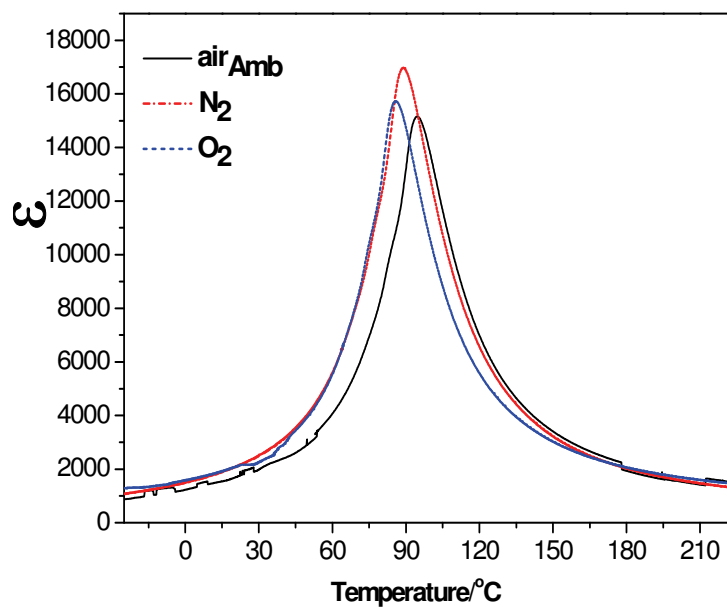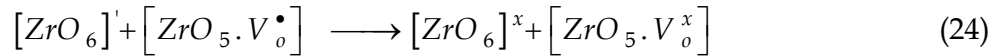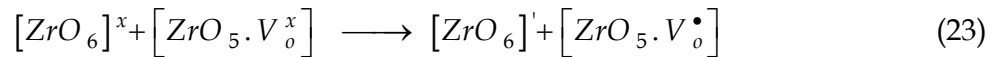

Fig. 17. Temperature dependence of dielectric permittivity at 10 kHz for BZT10:2V ceramics sintered at 1200 °C for 2 hours using air; O_2 and N_2 atmospheres.

The piezoeletric behavior at room temperature is shown in Figure 18a-c. Butterfly-shaped strain versus electric fields can be observed for different sintering atmospheres. The difference in the strain behavior might be attributed to different domain configurations. As usually observed in the relaxor-based "soft" piezoelectric materials, the hysteresis at low fields is attributed to domain motions. In the present work, the hysteresis could also be associated with the domain reorientation, which is prominent for a sample with a multidomain state. Above 30 kV/cm, the hysteresis-free strain is observed, implying a poling state free of domain wall motions induced by the high external electric fields. At 60 kV/cm, the highest electric field in the work, the piezoeletric coefficient is maximum. The oxidant and reducing atmosphere increase the piezoeletric behaviour in part due to domain reorientation. Beyond that point, it is possible that a modest bias field results in the transition from asymmetric to symmetric phase.

Inset shows the piezoforce microscopy of the BZT10:2V ceramics sintered under the air; O_2 and N_2 atmospheres. This field-induced phase transition may be ascribed to the pinching effect, that is, the consequent decrease in free energy difference among polymorphic phases.
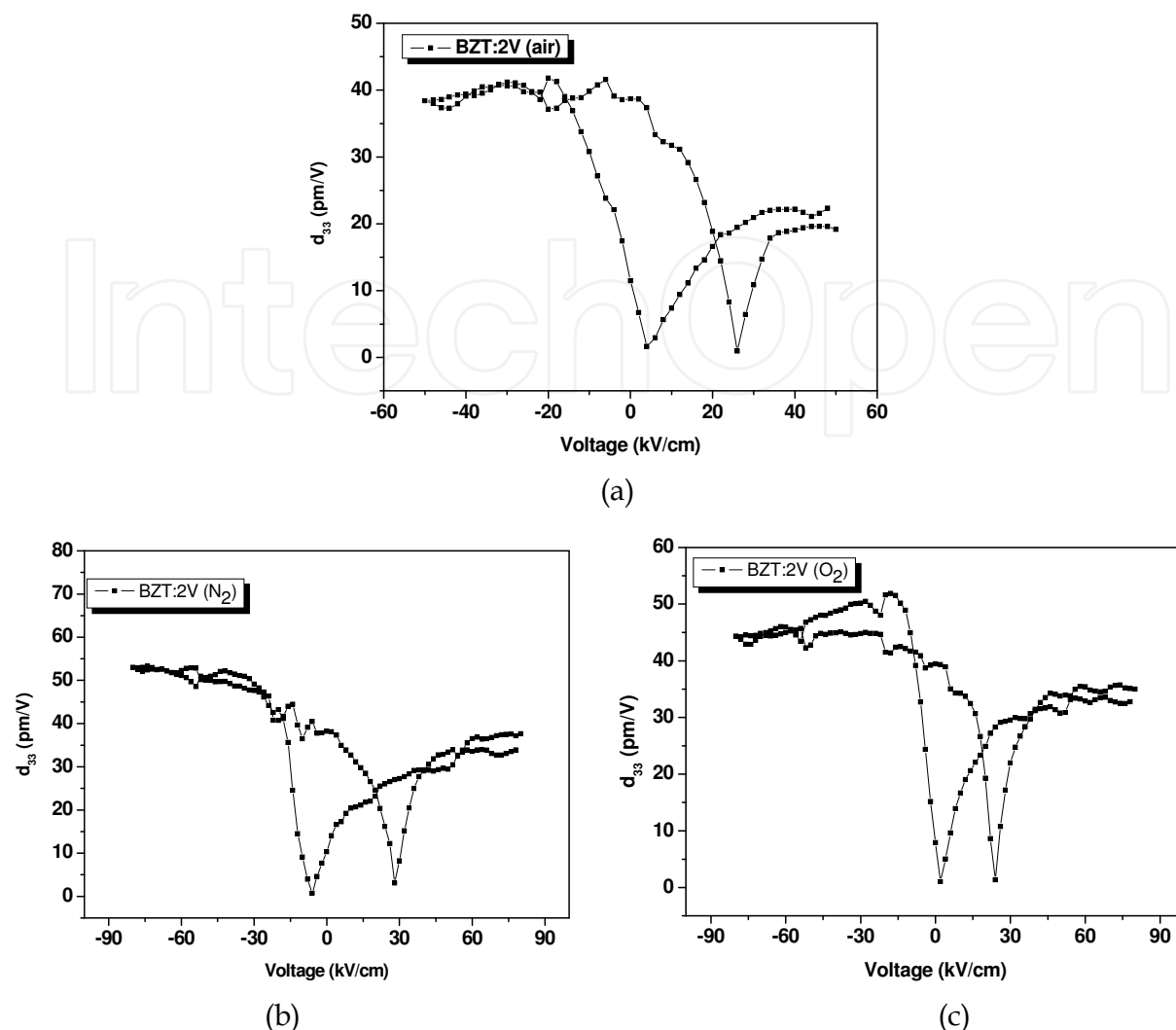
(a)

(b)

(c)

Fig. 18. Butterfly-shaped strain versus electric fields at room temperature for BZT10:2V ceramics sintered at 1200 °C for 2 hours using air; O_2 and N_2 atmospheres.

A careful inspection of the d_{33} -E plots reveals that there are two apparent linear regions at low fields (E<30 kV/cm) and high fields (E>70 kV/cm) and one transition region. That corresponds to domains reorientation induced by external electric fields. It is shown that BZT10:2V ceramic sintered in nitrogen atmosphere showed higher piezoeletric strain than the one sintered under air atmosphere. The piezoeletric coefficient was 43 pm/V, 40 pm/V and 30 pm/V for BZT10:2V ceramics sintered under nitrogen, oxygen and air atmospheres, respectively. This is a generally observed phenomenon in electronic ceramics, which might be attributed to the improved ceramic quality due to a small amount of impurity doping. It is shown that vanadium improves the piezoelectric strain. The improvement of piezoelectric response after doping can be associated with the better polarizability and the pinning effect.

6. Comparative study about behavior of BZT10, BZT10:2V and BZT10: 2W processed at different conditions

Figure 20 illustrates the XRD pattern for the BZT10, BZT10:2V and BZT10:2W ceramics sintered in a conventional furnace. The x-ray reflections show the single phase with a
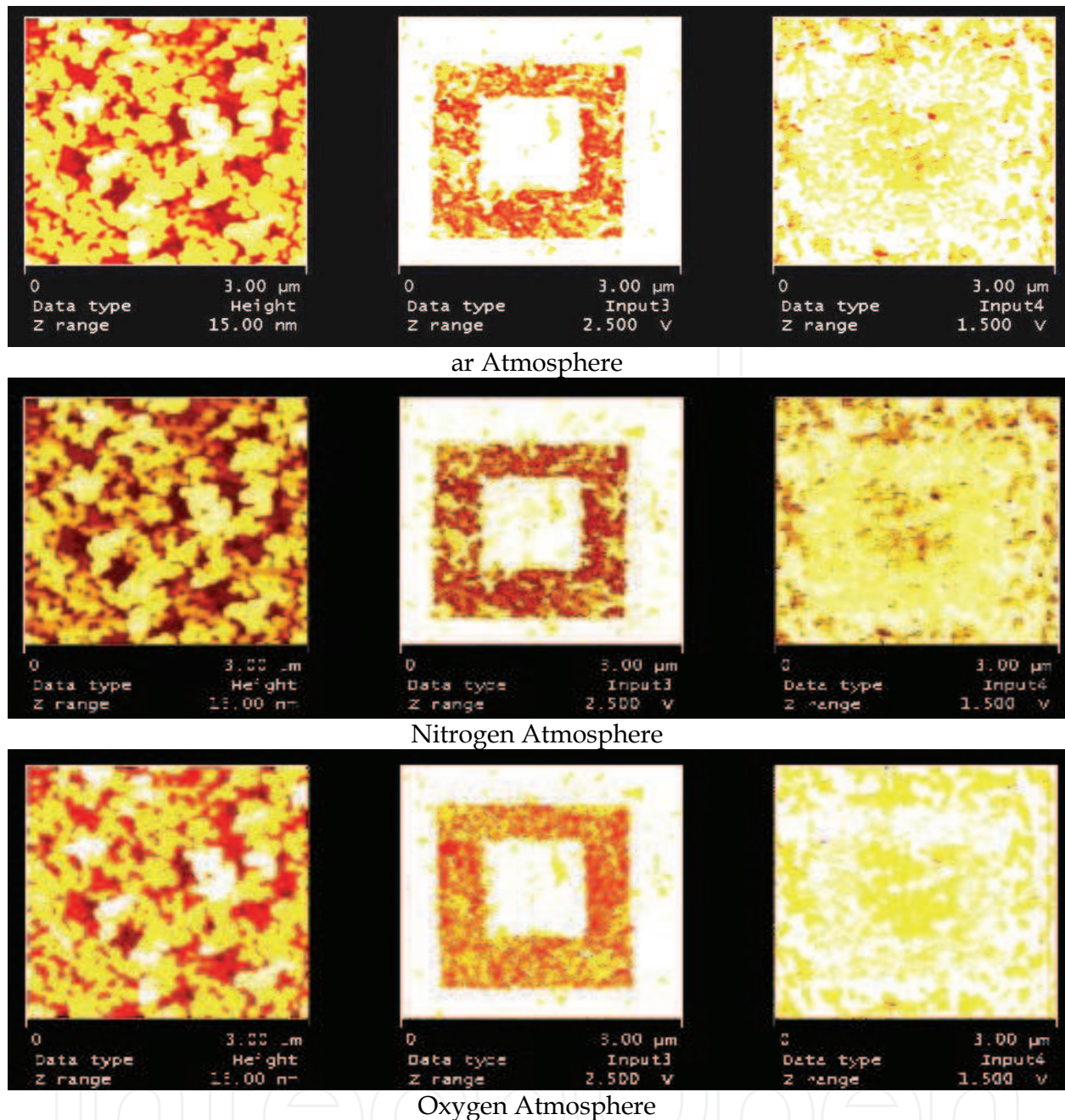
ar Atmosphere

Nitrogen Atmosphere

Oxygen Atmosphere

Fig. 19. Piezoelectric coefficient as function of voltage for BZT10:2V ceramics sintered at air; O_2 and N_2 atmospheres.

tetragonal perovskite structure was obtainedfor all the samples. This is a clear indication that V^{5+} and W^{6+} form a stable solid solution with the BZT10 lattice up to 2mol%. The peaks are indicative of a polycrystalline ceramic, mainly characterized by higher intense peak (hkl-110) at $2\theta = 31^o$. Vanadium and tungsten can either substitute titanium or zirconium in the lattice, depending on its concentration.

The substitution trend transition of dopant ions in the B-site of perovskite lattice can account for the influence of dopant on the sintering behavior of those ceramics, Figure 21. Due the fact that vanadium and tungsten play a role of donor in BZT10 lattice because it possesses a higher valence than Ti and Zr we noted a decrease of grain size, Figure 21b-c. This can be

explained by the suppression of oxygen vacancy concentration, which results in slower oxygen ion motion and consequently lower grain growth rate. As a result, there is a substantial improvement in the diffusion during sintering which facilitates the densification process.

Temperature dependence of dielectric permittivity and dielectric loss determined is shown in Figure 22 (a) and (b), respectively. The BZT10:2V ceramics present the highest permittivity (ε_r = 15111) at Curie temperature. The dielectric permittivity increases gradually with an increase in temperature up to the transition temperature (T_c), Curie point, and then decreases. A normal ferroelectric-paraelectric phase transition was obtained for the BZT10 and BZT10:2V ceramics, Figure 22(a). Above the transition temperature, dielectric permittivity follows the Curie-Weiss law. The V^{5+} center occupies the B-site of the ABO_3 perovskite lattice leading to a charged $[VO_6]^\bullet$ defect which is associated with a barium vacancy in a local barium cluster $[V_{Ba}'' O_{12}]$. In fully or partly ionic compounds vacancies are charge balanced by other defects forming an overall neutral system. It can be assumed that particle charge compensation takes place at a nearest-neighbor barium cluster site in the $[BaO_{12}]$ because the resulting coulomb interaction is the most important driving force. This assignment is in accordance with first-principles calculation (Anicete-Santos et al.,2005). Alternatively, like in BZT10:2V an equilibrium between "free" $[VO_6]^\bullet$ centers and $[VO_6]^\bullet$ + $[V_{Ba}'' O_{12}]$ associated defects can be reached. Hence, charge transport will be considerably hindered. In this way, $[VO_6]^\bullet$ + $[V_{Ba}'' O_{12}]$ affects dielectric properties due the charge gradient in the structure arising from both species.
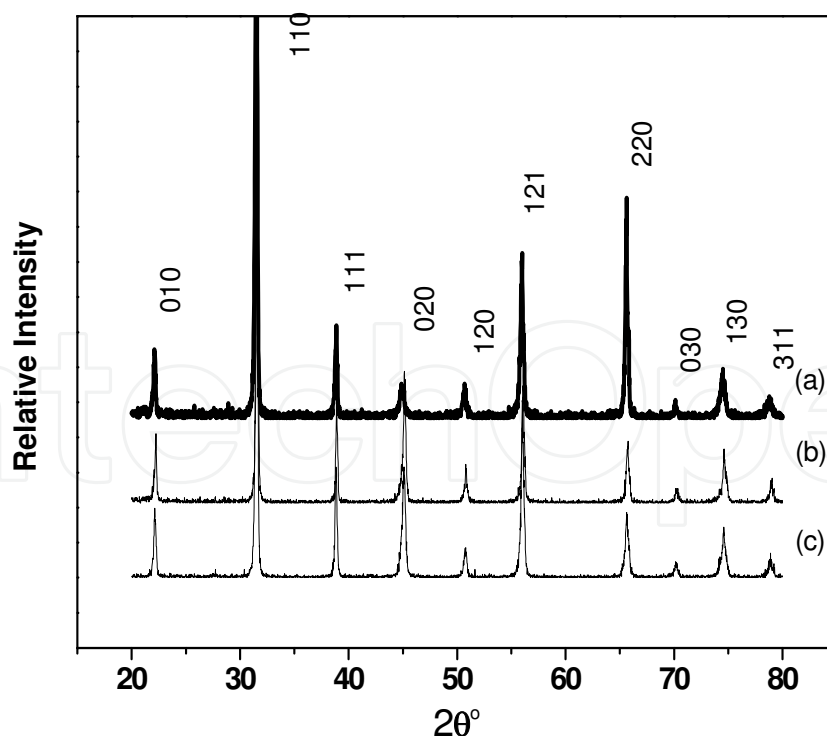

Fig. 20. X-ray diffraction data for ceramics sintered in a conventional furnace at different temperatures. (a) BZT10 -1550°C for 4 hours; (b) BZT10:2V- 1350°C for 4 hours; (c) BZT10:2W -1200°C for 2 hours.
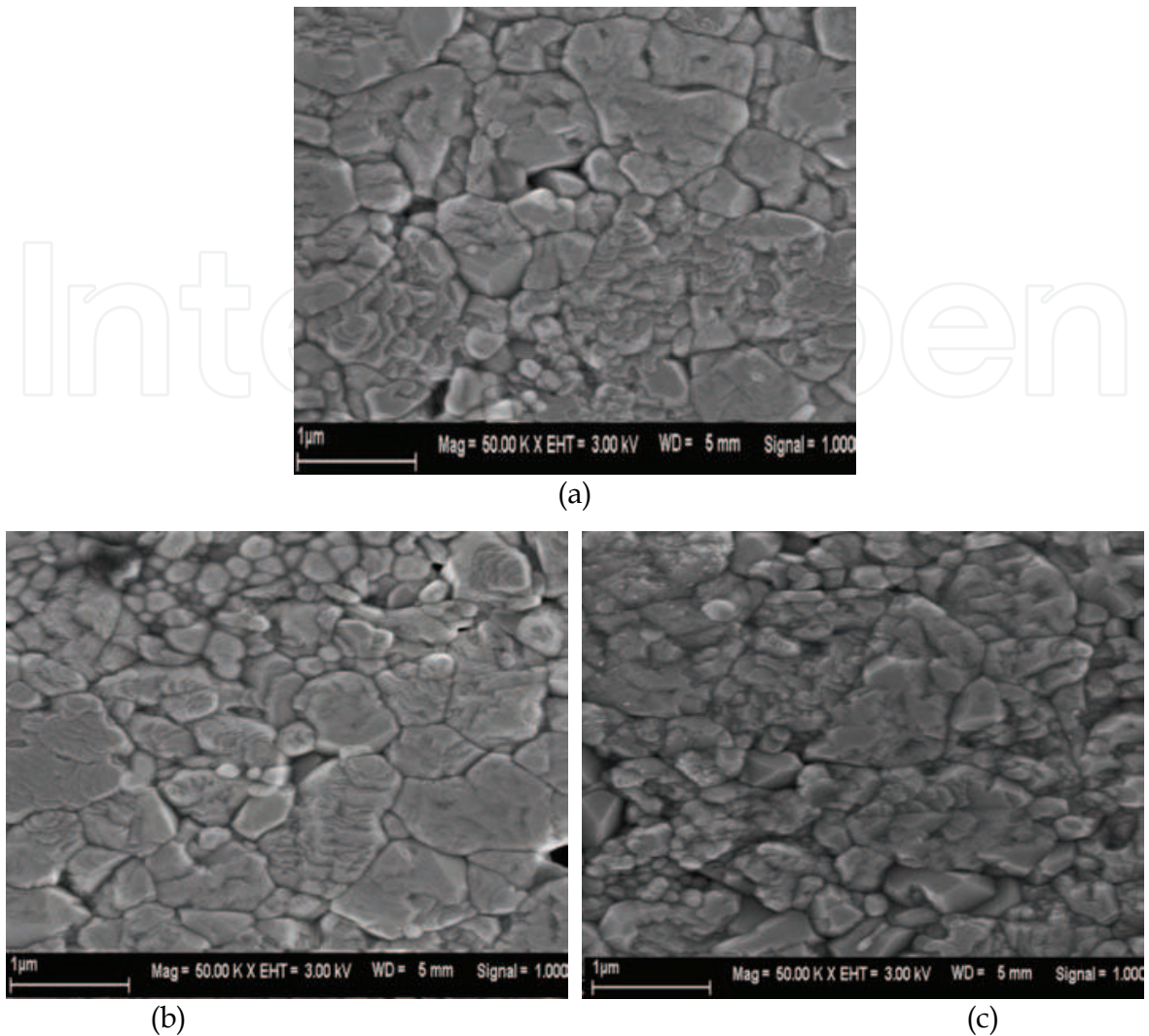
(a)

(b)

(c)

Fig. 21. Micrographies of the pellets ceramics sintered in a conventional furnace at different temperatures. (a) BZT10 -1550°C for 4 hours; (b) BZT10:2V- 1350°C for 4 hours; (c) BZT10:2W -1200°C for 4 hours;

That creates electron and hole polarons that can be designed as Jahn-Teller bipolarons, improving dielectric behavior due the charge trapping. For the BZT10:2W ceramic the dielectric anomaly is quite broad, covering the temperature range over 66°C. This compound exhibits diffuse dielectric permittivity anomalies around T_m. It can be also noticed that the maximum of dielectric permittivity ε_m and the corresponding maximum temperature, T_m, depend on the dopant. The magnitude of the dielectric permittivity decreases in this case, and the Curie temperature shifts toward lower temperature. This indicates that the dielectric polarization is of relaxation type in nature. The region around the dielectric peak is broadened due to a disorder in the cations arrangement in one or more crystallographic sites of the structure. Large differences in the B valence results in a strong tendency of disorder in one or more crystallographic sites of the structure leading to a microscopic heterogeneity in the compounds, with different Curie points. According to (Wu et al. 2002), the dielectric permittivity consists of contributions of ionic and atomic polarization only. Since the ionic radius of W^{6+} is smaller than that of Zr^{4+} and Ti^{4+}, increasing the amount of W^{6+} would lead to a reduced contribution of overall atomic

polarization. The incorporation of tungsten ions into BZT10 structure would introduce some cationic vacancies to maintain the electroneutrality. These cationic vacancies also influence the dielectric permittivity, resulting in a reduced Curie point and decrease stability of perovskite structure. The relatively larger ionic radius of the B ion enhances the thermal stability of the BO_6 octahedra, when compared to Ti or Zr. Therefore, tungsten influences the BZT10 in the following way: Acting by repulsion with their next nearest neighbors. This results in an increase of a and reduction of c parameters of tetragonal phase. As a consequence, the BO_6 volume octahedron increases and consequently decreasing its stability which results in a reduction of T_c. The Figure 22b shows the temperature dependence of dielectric loss determined at 10 kHz. A small peak just below the Curie temperature was observed. At lower temperatures, a small temperature dependence of dielectric loss was observed while at elevated temperatures, vanadium stabilizes the dependence. The possible formation of dipole complexes may result in a reduced dielectric loss at elevated temperatures. This reflects that good insulation resistance was maintained at high temperatures, which is important for high temperature piezoelectric applications. The dielectric losses at low temperature appear to be stable but sensitive at high temperatures. The higher value of dielectric loss at elevated temperatures may be due to transport of ions with higher thermal energy. The sharp increase in dielectric loss may be due to the scattering of thermally activated charge carriers and the presence of defects. At higher temperature the conductivity begins to dominate, which in turn is responsible for the rise in dielectric loss that is associated with the loss by conduction. Also at high temperature (paraelectric phase) the contribution of ferroelectric domain walls to dielectric loss decreases. This behavior was also observed in some similar types of compounds.
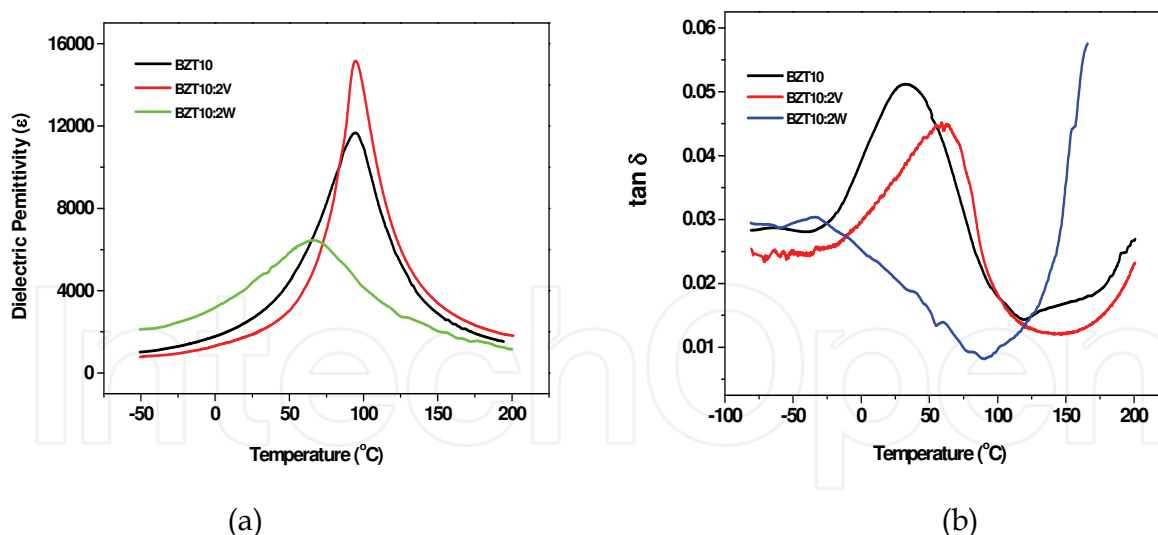

Fig. 22. Temperature dependence of dielectric permittivity (a); dielectric loss (b) for BZT10, BZT10:2V and BZT10:2W ceramics. The measurements were performed at 10 KHz

For a normal ferroelectric the Curie-Weiss law is followed :

$$1/\varepsilon = (T - T_o)/C \, (T > T_C)$$

(27)

where T_0 is the Curie temperature and C is the Curie-Weiss constant.

Figure 23 shows the inverse of dielectric permittivity as a function of temperature measured at 10 kHz. The fitting parameters for the BZT10, BZT10:2V and BZT10:2W were extracted from equation 27 and are C = 6.8x10⁻⁶ , T_0 = 98°C, C = 5.2x10⁻⁶ , T_0 = 93°C and C = 0.65x10⁻⁶, T_0 = 75°C , respectively (Table 1.). It is seen that the dielectric permittivity of BZT and BZT:2V ceramics follows the Curie-Weiss law at temperatures much higher than the $T_{\varepsilon m}$ (95 and 66 °C at 10 kHz).

Deviation from the Curie-Weiss law can be defined by

$$\Delta T_m = T_{cw} - T_{\varepsilon m} \tag{28}$$

where T_{cw} is a temperature at which ε starts to deviate from the Curie-Weiss law. Here, T_m = 95°C. In the literature, (Drougard & Huibregtse2010) a modified Curie-Weiss law was proposed to describe the diffuseness of the phase transition as

$$1 / \varepsilon - 1 / \varepsilon_m = (T - T_{\varepsilon m})^\gamma / C_1 \tag{29}$$

where γ and C_1 are assumed to be constant, and 1 < γ < 2. The parameter γ gives information on the character of the phase transition: For γ = 1, a normal Curie–Weiss law is obtained, γ = 2 describe a complete diffuse phase transition (Uchino et al.,1982) . The limiting values γ = 1 and γ = 2 reduce the expression to the Curie-Weiss law valid for the case of a normal ferroelectric and to the quadratic dependence valid for an ideal ferroelectric relaxor, respectively (Sinclair et al., 2002). From Figure 23, we obtained the parameter γ by fitting to the experimental data. The obtained values are for the BZT, BZT:2V and BZT:2W equal to 1.5, 1.4 and 2.0 respectively.The dipolar relaxation is clearly visible in the high frequency region. However, the low frequency region is dominated by the presence of grain boundary capacitances and likely the presence of deep trap states related to the Schottky-type barriers, which contribute to the total barrier-layer capacitive response of polycrystalline samples. With regard to the improvement in the dielectric properties, it can be inferred that both dopants exert a particularly marked influence on the grain's internal domain. Hence, they are able to increase the number of "active" domains, so that the cause of the strong increase in the dielectric properties is here mainly related to the number of active internal domains. The chemistry of dielectric internal domains most likely depends on the type of dopant to increase its effectiveness. In the particular context reported here, the grain boundary contribution is lower than the total dielectric response. For instance, the contribution of the grain boundary effect is more effective in the case of the sample modified with vanadium. In the case of the sample modified with tungsten, the contribution is not so significative and the total dielectric response decreased.

The piezoelectric behavior at room temperature is shown in Figure 24. The topography (TP), out-of-plane (OP) and in-plane (IP) piezoresponse images of the as-grown samples after applying a bias of -12V, on an area of 2 μm x 2 μm, and then an opposite bias of + 12V in the central 1 μm x 1 μm area. To obtain the domain images of the ceramics, a high voltage that exceeds the coercive field was applied during scanning. The contrast in these images is associated with the direction of the polarization. The PFM image indicates that the perpendicular component of polarization can be switched between two stable states: bright and dark contrast inside and outside of the square region. Higher PFM magnification images showed that the regions without piezoresponse exhibit a strong contrast in the PFM images. The white regions in the out-of-plane PFM images correspond to domains with the polarization vector oriented toward the bottom electrode hereafter referred to as down
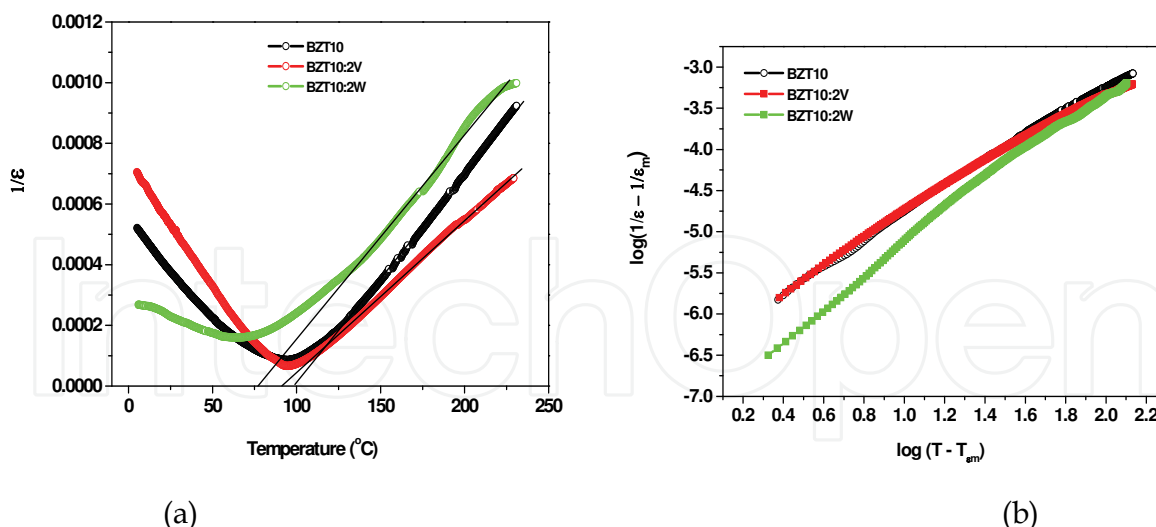
(a) (b)

Fig. 23. The inverse dielectric permittivity $(10000/\varepsilon)$ as a function of temperature at zero electric field (a) ; $\ln(1/\varepsilon-1/\varepsilon_m)$ as a function of $\ln(T-T_m)$ (b); for BZT10, BZT10:2V and BZT10:2W ceramics.

Samples	BZT10	BZT10:2V	BZT10:2W
$T_o(°C)$	97.8	92.9	74.9
C $(x10^{-6})$	6.8	5.2	6.5
$T_{cw}(°C)$	125.5	113.4	131.5
$\Delta T_m = T_{cw} - T_{\varepsilon m}(°C)$	27.7	20.5	65.2
$T_{\varepsilon m}(°C)$	94.7	94.6	66.3
εm	11670	15160	6420
γ	1.5	1.4	2.0
$\Delta T_m = T_{\varepsilon m}(100KHz) - T_{\varepsilon m}(1KHz)(°C)$	571.6	1124.4	235

Table 1. The Curie-Weiss temperature (T_0); Curie-Weiss constant (C); temperature above which the dielectric permittivity follows the Curie-Weiss law (T_{cw}); temperature of maximum dielectric permittivity $(T_{\varepsilon m})$; maximum dielectric permittivity (ε_m); and diffuseness constant (γ).

polarization (Figures 24b, e and h) while the dark regions correspond to domains oriented upward referred to as up polarization. Grains which exhibit no contrast change is associated with zero out-of-plane polarization. A similar situation was observed when a positive bias was applied to the samples. We noticed that some of the grains exhibit a white contrast associated to a component of the polarization pointing toward the bottom electrode. On the other hand, in the in-plane PFM images (Figures 24 c, f and i) the contrast changes were associated with modifications in the in-plane polarization components. In this case, the white contrast indicates polarization pointing to the positive direction of the y-axis while dark contrast is given by in-plane polarization components pointing to the negative part of the y-axis.
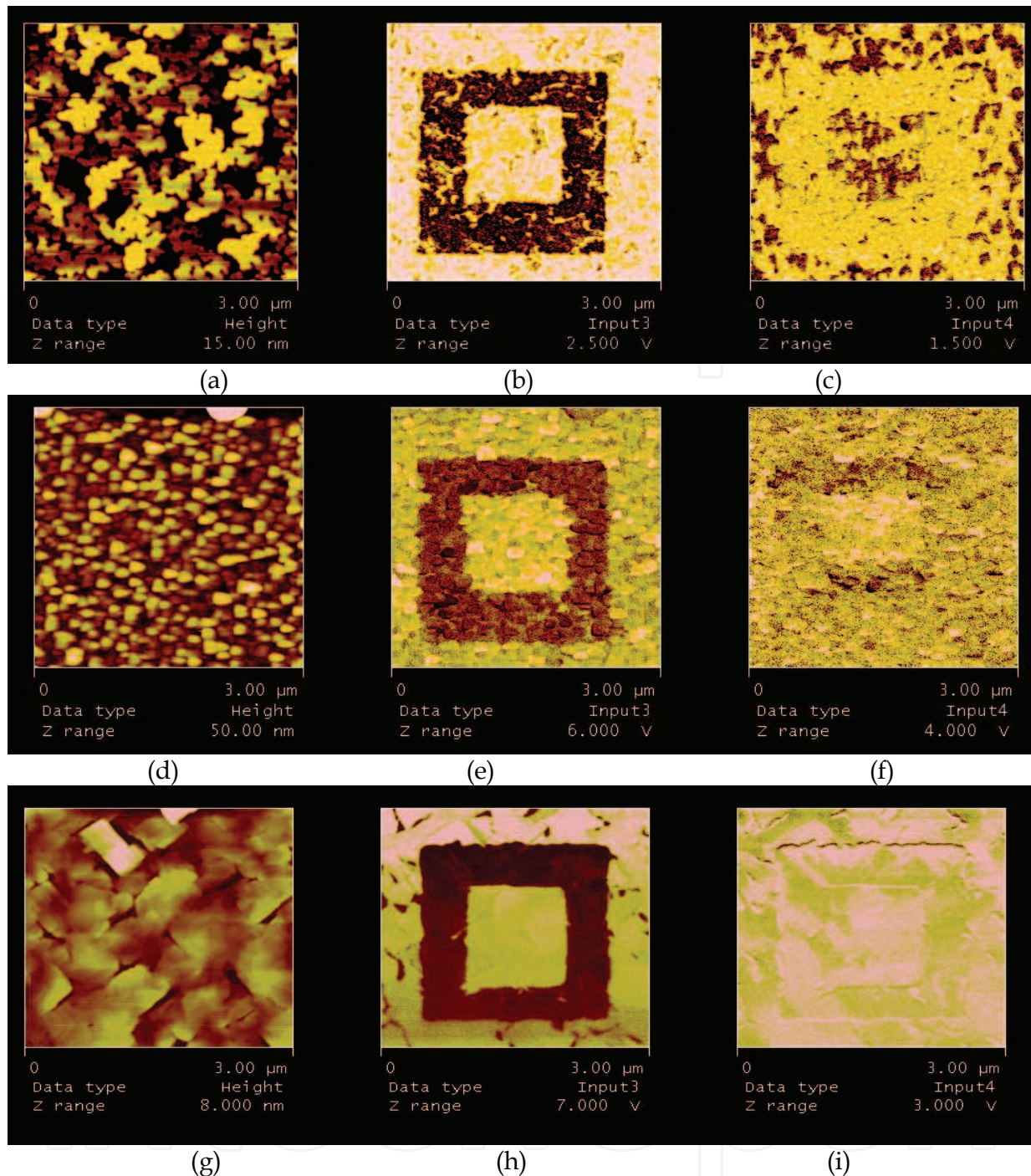
Fig. 24. Topography (TP), Out-of-plane (OP) and In-plane (IP) PFM images of (a) BZT10 (TP), (b) BZT10 (OP), (c) BZT10 (IP), (d) BZT10:2V (TP), (e) BZT10:2V (OP), (f) BZT10:2V (IP), (g) BZT10:2W (TP), (h) BZT10:2W (OP) and (i) BZT10:2W (IP)ceramics.

Considering the polycrystalline nature of our samples the effective piezoelectric coefficient depends on grain orientation. Therefore, as expected the piezoelectric response improves with addition of donor dopant due to the reduction of strain energy and the pinning effect of charged defects. The difference in the piezoresponse behavior might be attributed to different domain configurations. As usually observed in the relaxor-based ''soft'' piezoelectric materials, the piezoresponse at low fields is attributed to domain motions. In

Influence of Dopants, Temperature and Atmosphere of
Sintered on the Microstructure and Behavior of Lead Free Ceramics
207

the present work, the high PFM contrast could also be associated with the domain reorientation, which is prominent for a sample with a multidomain state. Donor dopants such as vanadium and tungsten improve the piezoelectric response due the better polarizability and the pinning effect. PFM measurements also reveal a clear piezoelectric contrast corresponding to antiparallel domains on all locations tested. There is no reduction in the amplitude of the measured vibrations which is indicative that this phase is still polar and electric field-induced polarization switching still exists. Also, we noted that some of the crystallites apparently have not been switched and still exhibit a positive piezoresponse signal. This result, which can be explained by strong domain pinning in these crystallites, is direct experimental proof that repeated switching results information of unswitchable polarization, which, in turn, leads to the degradation of switching characteristics. Finally, it is shown in the PFM images that BZT10:2V and BZT10:2W ceramics showed higher piezoelectric strain than the BZT10. The piezoelectric coefficient was 43 pm/V, 40 pm/V and 30 pm/V for BZT10:2V, BZT10:2W and BZT10 ceramics, respectively (not shown in the text). This is a generally observed phenomenon in electronic ceramics, which might be attributed to the improved ceramic quality due to a small amount of impurity doping.

7. Conclusions

Single phase BZT powders were obtained from mixed oxide method at 1200°C for 2 hours. Raman spectroscopy indicated a change in the crystal structure with the increase of zirconium content. The transition temperature (ferroelectric to paraelectric phase) was found to be systematically reduced for Zr content equal to 15.0 mol.%. In this case, a typical relaxor behavior was observed. A decay in the dielectric permittivity and remnant polarization with the increase of zirconium content is indicative of changes in crystal structure and predominance of relaxor behaviour.

$Ba(Zr_{0.10}Ti_{0.90})O_3$:2V (BZT:2V) ferroelectric ceramics modified with vanadium were prepared from powders synthesized using the mixed oxide method. Single phase ceramics crystallized in a tetragonal structure was attained at 1350°C for 4 hours. Dielectric properties of BZT:2V ceramics have been investigated and at 10 KHz the maximum dielectric permittivity reached was 15000 at a Curie temperature of 94 °C. Dielectric constant of BZT:2V ceramics follows the Curie-Weiss law at temperatures much higher than T_{em}. The remanent polarization (Pr) and coercive electric field (Ec) of BZT:2V ceramics was found to be 8.5 $\mu C/cm^2$ and 2 kV/cm, respectively. The very high-dielectric constant and high at low temperatures of this material are promising for some practical applications.

The dielectric and piezoelectric properties of BZT10 based ceramics depends on the donor dopant. Single phase BZT10, BZT10:2V and BZT10:2W ceramics crystallized in a tetragonal structure was attained. Micrographies reveal that both dopants suppress the oxygen vacancy concentration which results in slower oxygen ion motion and consequently lower grain growth rate. A maximum dielectric constant was obtained for the BZT10:2V ceramics at a Curie temperature of 95°C.

The maximum sintering temperature is reduced after tungsten addition due to generation of oxygen vacancies. The tungsten doped BZT powders consist of soft agglomerates which were completely broken during milling process and densified at lower temperatures. Tungsten addition leads to the distortion of the perovskite lattice leading to typical relaxor behaviour. Dielectric properties have been investigated and a maximum dielectric permittivity for the undoped BZT10 reached 11500 at Curie temperature of 93°C. The

dielectric permittivity is reduced and shifted to lower temperatures up to a tungsten content of 2 mol%. Room-temperature EPR spectrum evidenced hyperfine bands resulting from interaction between species with unpaired electrons with species which present complex vacancies. The BZT10:2W ceramic showed a relaxor-like behaviour near phase transition which can be useful for low temperature capacitor applications.

Dielectric permittivity of BZT10 and BZT10:2V ceramics follows the Curie-Weiss law at temperatures much higher than $T_{\varepsilon m}$. BZT10:2W ceramic showed a relaxor-like behavior near phase transition based on empirical parameter γ. In BZT10, the movement of Ti^{4+} and Zr^{4+} ions reduces the space charge compensation leading to a low piezoresponse signal. Meanwhile, BZT:2V and BZT10:2W ceramics exhibited excellent piezoelectric We report the advances in the dielectric and piezoelectric properties of vanadium and tungsten doped BZT10 ceramics prepared by the mixed oxide method by using dielectric spectroscopy analyses and piezoresponse force microscopy. Ceramics with good electrical properties were obtained confirming the possibility of application of ferroelectric perovskite materials lead free such as barium zirconium titanate.

The effect of annealing atmosphere (air, N_2 and O_2) on the electrical properties of BZT10:2V was investigated. The results show that ceramic sintered in nitrogen atmosphere presents superior dielectric behavior at room temperature. The dielectric permittivity measured at a frequency of 10 kHz was equal to 16800 with dielectric loss of 0.030. The BZT10:2V ceramic sintered in air atmosphere restricting the movement of Ti^{4+} and Zr^{4+} ions and thus reducing the space charge compensation leading to a low piezoresponse. Meanwhile, BZT10:2V ceramic sintered in oxygen and nitrogen atmospheres exhibited excellent piezoelectric properties indicating that the environment of the oxygen ions is quite different from one sample to another. The piezoelectric coefficient is strongly improved by sintering the sample under nitrogen atmosphere. In this way, we reveal that BZT:2V ceramic sintered under nitrogen atmosphere can be useful for practical applications, including nonvolatile digital memories, spintronics and data-storage media.

8. Acknowledgments

9. References

Abraham, M.M.; Boatner, L.A. & Aronson, M.A. (1986), EPR observations of trivalent titanium in orthophosphate single crystals, *J.Chem. Phys,*vol. 85, n 1, pp. 1–6. ISSN 0021-9606.

Anicete-Santos, M. Cavalcante, L.S. Orhan, E. Paris, E.C. Joya, M.R. de Lucena P.R., Pizani, P.S. Leite, E.R. Varela, J.A. Longo, E. The role of structural order–disorder for visible intense photoluminescence in the $BaZr_{0.5}Ti_{0.5}O_3$ thin films, Chem. Phys, Vol.316, No 4 (2005). pp. 260-266. ISSN0301-0104.

Bolten, D. Bouger, U. Schneller, T. Grossnam, M. Lose, O., & Waser, R., Reversible and irreversible processes in donor-doped $Pb(Zr,Ti)O_3$. *Appl. Phys. Lett.*, Vol. 77, No 23, (2000). pp.3830–3832, ISSN 0003-6951.

Böttcher, C. J. F. & Bordewijk, P., (1992) Theory of Electric Polarization: Dielectrics in Time-Dependent Fields (Elsevier, Amsterdam) Vol. II.

Caballero, A. C.; Fernández, J. F.; Villegas, M. ; Moure, C.; Durán, P. ; Florian, P. & Coutures, J.P. (1998). Intermediate Phase Development in Phosphorus-Doped Barium Titanate. *J. Am. Ceram. Soc.,* 20 dec , vol. 8, n 6, pp.1499-1505, ISSN 0002-7820.

Carg, A. & Goel, T.C. Dielectric properties of NiZn ferrites by the precursor method, *Mater. Sci. Eng. B.*, Vol. 60, No 2, (1999). pp. 156–160, ISSN 0921-5107.

Chen, I-W. and Xue, L.A. Development of Superplastic Structural Ceramics. *J. Amer. Ceram. Soc.,* Vol. 73, No 9, (1990). pp. 2585-2609, ISSN 002-7820.

Chen, A.; Yu,Z.; Cross,L. E.; Guo, R. Y. & Bhalla, A. S., (2001). Dielectric relaxation and conduction in SrTiO3 thin films under dc bias. *Appl. Phys. Lett.*, vol. 79, n 8, pp. 818-820, ISSN 0003-6951.

Cheng, Z-Y. Katiyar, R. S. Yao, X. Bhalla, A. S. Temperature dependence of the dielectric constant of relaxor ferroelectrics, *Phys. Rev. B.,* Vol. 57, No 14, (1998). pp. 8166-8177, ISSN 0163-1829.

Courtens, E.. Vogel-Fulcher Scaling of the Susceptibility in a Mixed-Crystal Proton Glass. *Phys. Rev. Lett.,*Vol. 52, No 1, (1984). pp. 69-72, ISSN 0031-9007.

Cross, L. E. Relaxor ferroelectrics. *Ferroelectrics,* Vol. 76, n. 3-4, (1987). pp. 241-267, ISSN 1563-5228.

Dixit, A.; Majumder, S. B.; Dobal, P. S.; Katiyar, R. S. & Bhalla, A. S. (2004). Phase transítion studies of sol–gel deposited barium zirconaté titanaté thin films. Thin Solid Films, Vol. 447-448, pp. 284–288, ISSN 0040-6090

Dmowski, W. Akbas, M.K. Davies, P.K. Egami, T.Local structure of Pb(Sc1=2,Ta1=2)O₃ and related compounds, *J. Phys. Chem. Solids.*, Vol. 61, No 3, (2000) pp.229–237, ISSN 0022-3697.

Dobal, P. S.; Dixit, A.; Katiyara, R. S. (2010). Micro-Raman scattering and dielectric investigations of phase transition behavior in the BaTiO3–BaZrO3 system. *J. Appl. Phys,* Vol. 89, pp. 8085-8091, ISSN 0021-8979.

Domenico, M. D. Jr.; Wemple, S. H.; Porto, S. P. S. & Buman, P. R. Raman spectrum of single-domain BaTiO3. *Phys. Rev.*, v. 174, (1968) p. 522-530,

Fang, T. T. and Shiau, H. K. Mechanism for Developing the Boundary Barrier Layers of CaCu₃Ti₄O₁₂. *J. Am. Ceram. Soc., Vol.* 87, No 11, (2004). pp. 2072-2079, ISSN 1551-2916.

Farhi, R. Marssi, M. El. Simon, A. & Ravez, J. A Raman and dielectric study of ferroelectric Ba(Ti$_{1-x}$Zr$_x$)O₃ ceramics, *Eur. Phys. J. B.*, Vol. 9, No 4, (1999). pp. 599–604, ISSN 1434- 6028.

Fouskova, A. Cross, L. E. Dielectric properties of Bismuth Titanate. *J. Appl. Phys.,* Vol. 41, No 7, (1970). pp. 2834-2838, ISSN 1089-7550.

Hennings, D. & Sehnell, A. Diffuse Ferroelectric Phase Transitions in Ba(Ti$_{1-y}$Zr$_y$)O₃ Ceramics. *J.Am. Ceram. Soc,* Vol. 65, No 3, (1982) pp. 539-534, ISSN 0002-7820.

Hoffmann, S. Waser, R. Control of the morphology of CSD-prepared (Ba, Sr) TiO₃ thin films. *J. Eur. Ceram. Soc.,* Vol. 19, No 6-7, (1999). pp. 1339-1343, ISSN 0955-2219

Jin, D., Hing,P., & Sun, C.Q. Intense and stable blue-light emission of Pb(Zr$_x$Ti$_{1-x}$)O₃, *Appl. Phys. Lett.*, *Vol.* 79 (2001). pp. 1082–1084. ISSN 0003-6951.

Jonscher, A. K. Dielectric characterisation of semiconductors. *Solid-State Electron.,* Vol. 33, No 6, (1990). pp.737-742, ISSN 0038-1101.

Kell, R.C. Hellicar,N.J. Structural transitions in barium titanate- zirconate transducer materials. Acusticu., Vol. 6, (1956). pp 235–238, ISSN 1610-1928.

Kreisel, J.; Bouvier, P.; Maglione, M.; Dkhil, B. & Simon, A. High-pressure Raman investigation of the Pb-free relaxor Ba(Ti0.65Zr0.35)O3. *Phys. Rev. B*, v1. 69 (2004)p. 092104.

Landolt Bornstein, (1981) Ferroelectric: oxides, New series, Group III, Vol. 16a Berlin, Heidelberg, New York : Springer,

Liu, S. F. Park, S. E. Shrout, T. R. and Cross, L. E. Electric field dependence of piezoelectric properties for rhombohedral $0.955Pb(Zn_{1/3}Nb_{2/3})O_3$-$0.045PbTiO_3$ single crystals. J. Appl. Phys., Vol. 85, No 1, (1999). pp. 2810-2814, ISSN 1089-7550.

Lines, M.E. & Glasss, A.M. (1977) *Principles and applications of ferroelectrics and related materials*, Oxford University Press, Oxford

Marques, L.G.A., Cavalcante,L.S., Simões,A.Z, Pontes, F.M., Santos-Junior,L.S., Santos,M.R.M.C., Rosa,I.L.V., Varela,J.A.,& Longo, E. ,Temperature dependence of dielectric properties for $Ba(Zr_{0.25}Ti_{0.75})O_3$ thin films obtained from the soft chemical method, *Mater. Chem. Phys*, Vol. 105, No 2, (2007). pp. 293–297, ISSN 0254-0584.

Merz, W.J. The effect of an electric field on the transitions of barium titanate. *Phys. Rev.,* Vol. 91, (1953). pp. 513-517, ISSN 0031-9007

Miura, S. Marutake, M. Unoki, H. Uwe, H. Sakudo, T.Composition Dependence of the Phase Transition Temperatures in the Mixed Crystal Systems near $SrTiO_3$. J. Phys Soc Jpn., Vol. 38, No 1, (1975).pp. 1056-1060, ISSN 0031-9015.

Moura, F. Simões, A. Z. Cavalcante, L. S. Zampieri, M. Zaghete, M. A. Varela, J.A. & Longo, E. Strain and vacancy cluster behavior of vanadium and tungsten-doped. *Appl. Phys. Lett.,* Vol. 92, No 3, (2008). pp. 032905-032907, ISSN 0003-6951.

Moura,F., Simões,A.Z., Aguiar,E.C., Nogueira,I.C., Zaghete,M.A., Varela, J.A. & Longo, E., Dielectric investigations of vanadium modified barium titanate zirconate ceramics obtained from mixed oxide method, *J. Alloys and Compds*, Vol. 479, No 4, (2009). pp. 280–283, ISSN 0254-0584.

Moura,F., Simões,A.Z., Paskocimas, C.A., Zaghete,M.A., Longo E. & Varela,J.A., Temperature Dependence of Electrical Properties of BZT:2V ceramics, *Mater. Chem. Phy,* Vol. 479, No 3 (2009). pp. 280–283, ISSN 0254-0584.

Neirman, S. M., The Curie Point Temperature of $Ba(Ti_{1-x}Zr_x)O_3$ Solid Solution., *J. Mater. Sci,* Vol. 23, No 11, (1988). pp. 3973-3980, ISSN 1573-4803.

Paik, D. S. Park, S. E. Wada, S. Liu, S. F. and Shrout, T. R. "E-field induced phase transition in ferroelectrics. *J. Appl. Phys.,* Vol. 5, No 2, (1999). pp. 1080-1083, ISSN 1089-7550.

Park, S. E. and Shrout, T. R. Ultrahigh strain and piezoelectric behavior in relaxor based ferroelectric single crystals. *J. Appl. Phys.,* Vol. 82, No 4, (1997). pp.1804-1815, ISSN 1089-7550.

Ravez J.& Simon A., "Raman spectroscopy and soft modes in the model ferroelastics", *Eur. Phys. J.: Appl. Phys.,* 11 (1997) 9–13.

Ravez, J. & Simon, A. (1997). The crystal *chemistry* of the higher tungsten oxides. *J. Solid State Chem,* Vol. 34, No 1, (1997). pp. 1199- 1203, ISSN 0022- 4596

Ravez, J. Simon, A. Spontaneous transition from relaxor to ferroelectric state in new lead-free perovskite ceramics. *Ferroelectrics., Vol.* 240, No 1, (1999). pp. 313-320, ISSN 1563-5228.

Ravez, J. Simon, A. Raman spectroscopy and soft modes in the model ferroelastics, *Eur. Phys. J: Appl. Phys.,* Vol. 11, No 3, (1997). pp. 9–13, ISSN 1089-7550.

Ravez, J. Simon, A. The crystal chemistry of the higher tungsten oxides, *J. Solid State Chem.*, Vol. 34, No 2, (1997). pp. 1199-1203, ISSN 0022-4596

Rehrig,P. W. Park, S. E. McKinstry, S. T. Messing, G. L. Jones, B. and Shrout, T.M. Piezoelectric properties of zirconium-doped barium titanate single crystals grown by templated grain growth. J. Appl. Phys., Vol . 86, No 3, (1999). pp. 1657-1651, ISSN 1089-7550.

Scott, J. F. Soft-mode spectroscopy: Experimental studies of structural phase transitions. *Rev. Mod. Phys*, Vol. 46, No 1, (1974) pp. 83-128, ISSN 0034-6861

Shannigrahi, R. Choudhary, R.N.P. Acharya, N. Electrohydrodynamic instability in 8CB (4'-n-octyl-4-cyanobiphenyl) liquid crystal, *Mater. Sci. Eng. B.*, Vol. 56, No 2, (1999). pp. 31–35, ISSN 0921-5107.

Shannigrahi,R. , Choudhary, R. N. P. & Acharya,N. Phase transition in $Ba_5RTi_3Nb_7O_{30}$ (R = Dy, Sm) ferroelectric ceramics, *Mater. Sci. Eng.*, B 56 (1999) 27-31.

Simões,A.Z., Ramirez,M.A., Riccardi,C.S., Ries, A., Longo,E., Varela,J.A.Influence of temperature on the dielectric and ferroelectric properties of bismuth titanate thin films obtained by the polymeric precursor method. *Materials Chemistry and Physics.*, Vol. 92, No 2-3 (2005) pp. 373–378, ISSN 0254-0584.

Sinclair,D. C. Adams, T. B. Morrison,F. D. West, A. R. $CaCu_3Ti_4O_{12}$: one-step internal barrier layer capacitance. *Appl. Phys.Lett.*, Vol. 80, No 1, (2002). pp. 2153-2155 , ISSN 0003-6951.

Smolensky, G.A. ; Bokov,V.A. ; Isupov,V.A. ; Krainik, N. N. & Pasynkov, R. E., (1984) Ferroelectrics and Related Materials (New York: Gordon and Breach), ISBN 10 – 2881241077.

Tagantsev, A. K. Glazounov, A.E. Mechanism of polarization response in the ergodic phase of a relaxor ferroelectric. *Phys. Rev. B.*, Vol. 57, No 1, (1998). pp.18-21, ISSN 0163-1829.

Takahashi, S. Effects of impurity doping in lead zirconate-titanate ceramics. *Ferroelectrics.*, Vol. 41, No 2, (1982). pp. 277–290, ISSN 0015-0193

Tang, X.G. Wang, J. Wang, X.X. Chan, H.L.W. Tunabilities of sol-gel derived Ba (Zr0.2Ti0.8)O3 ceramics. *Solid State Communications.*, Vol. 131, No 3, (2004). pp. 163–168, ISSN 0038-1098

Tsurumi, T. Yamamoto, Y. Kakemoto, H. Wada, S. Chazono, H. Kishi, H. Dielectric properties of $BaTiO_3$-$BaZrO_3$ ceramics under a high electric field. *J. Mater. Res.*, Vol. 17, No 2, (2002). pp. 755-759, ISSN 0884-2914.

Uchino, K. Nomura, S.Critical Exponents of the Dielectric Constants in Diffused-Phase-Transition Crystals. *Ferroelectr. Lett. Sect.*, Vol. 44, No 1, (1982) pp. 55-61, ISSN 1563-5228.

Veith, G. M., Greenblatt, M., Croft, M. and Nowik, I. Fawcett, I. D., Properties of the perovskites, $SrMn_{1-x}Fe_xO_{3-\delta}$ (*x*=1/3; ½; 2/3), Solid State Sciences, Vol. 2, Issue 8, 2000, pp.821-831

Wang, Y.L. Li, L.T. Qi, J.Q. Gui, Z.L. Low-Temperature Facile Template Synthesis of Crystalline Inorganic. *Mater. Chem. Phys.*, Vol. 76, No 3 (2002). pp. 250-254, ISSN 0254- 0584.

Weber, U. Greuel, G. Boettger, U. Weber, S. Hennings, D. Waser, R. Manufacturing Processes and Systems. *J. Am.Ceram. Soc.*, Vol. 84, No 4, (2001). 759-766.

WEBER, U.; GREUEL, G.; BOETTGER, U.; WEBER, S.; HENNINGS, D.; & WASER, R., Dielectric Properties of Ba(Zr,Ti)O$_3$-Based Ferroelectrics for Capacitor Applications, *J. Am. Ceram. Soc,* v. 84 (2001)p. 759–66

West, A. R. Adams, T. B. Morrison, F. D. Sinclair, D. C.'Novel High. Capacitance Materials: BaTiO$_3$:La and CaCu$_3$Ti$_4$O$_{12}$. J.Eur.Ceram. Soc., Vol. 24, No 6, (2004). pp. 1439-1448, ISSN 0

Wu,L.; Wei,C.; Wu,T. & Liu,H. Dielectric properties of modified PZT ceramics, *J. Phys. C: Solid State Phys.*, 16 (1983) 2803–2806.

Wu, L.; Wei,C. ; Wu, T. & Liu, H. "Effects of dye loading", *J. Phys. C: Solid State Phys.*, 16 (1983) 2803–2806.

Wu,Y.; Limmer, S.J. ; Chou,T.P. ; Nuguyen, C. & Guozhong, C. "Influence of tungsten doping on dielectric properties of strontium bismuth niobate ferroelectric ceramics", *J. Mater. Sci. Lett.*, 21 (2002) 947–949.

Xu, Y. H. 1991, *Ferroelectric Materials and their Applications*, Elsevier Science Publishers, Amsterdam.

Zhang, M.; Jin, Z.; Zhang,J.; Gou, X.; Yang, J.; Wang, X. & Zhang, Z. (2004). Effect of annealing temperature on morp hology, structure and photocatalytic behavior of nanotubed H$_2$Ti$_2$O$_4$(OH)$_2$, *J. Mol. Catal. A: Chem.*, vol. 217, pp 203–210
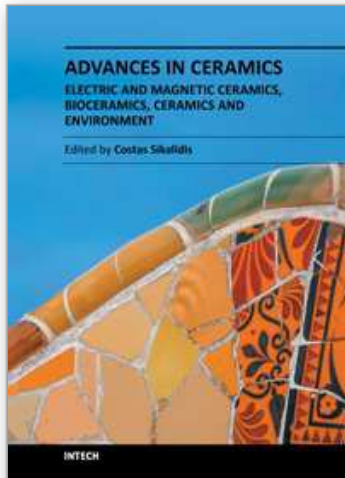
Advances in Ceramics - Electric and Magnetic Ceramics, Bioceramics, Ceramics and Environment

Edited by Prof. Costas Sikalidis

The current book consists of twenty-four chapters divided into three sections. Section I includes fourteen chapters in electric and magnetic ceramics which deal with modern specific research on dielectrics and their applications, on nanodielectrics, on piezoceramics, on glass ceramics with para-, anti- or ferro-electric active phases, of varistors ceramics and magnetic ceramics. Section II includes seven chapters in bioceramics which include review information and research results/data on biocompatibility, on medical applications of alumina, zirconia, silicon nitride, ZrO2, bioglass, apatite-wollastonite glass ceramic and b-tri-calcium phosphate. Section III includes three chapters in applications of ceramics in environmental improvement and protection, in water cleaning, in metal bearing wastes stabilization and in utilization of wastes from ceramic industry in concrete and concrete products.

How to reference

In order to correctly reference this scholarly work, feel free to copy and paste the following:

Maria A. Zaghete, Francisco Moura, Alexandre Z. Simões, José A.Varela and Elson Longo (2011). Influence of Dopants, Temperature and Atmosphere of Sintered on the Microstructure and Behavior of Lead Free Ceramics, Advances in Ceramics - Electric and Magnetic Ceramics, Bioceramics, Ceramics and Environment, Prof. Costas Sikalidis (Ed.), ISBN: 978-953-307-350-7, InTech, Available from:
http://www.intechopen.com/books/advances-in-ceramics-electric-and-magnetic-ceramics-bioceramics-ceramics-and-environment/influence-of-dopants-temperature-and-atmosphere-of-sintered-on-the-microstructure-and-behavior-of-le

INTECH

open science | open minds